Characterization of preserved remnants of the Pre-Pleistocene Saprolite on the Canadian Shield: Examples from Northeastern Minnesota.

A Thesis
SUBMITTED TO THE FACULTY OF THE UNIVERSITY OF MINNESOTA BY

Christa Noelle Wood

IN PARTIAL FULFILLMENT OF THE REQUIREMENTS FOR THE DEGREE OF MASTER OF SCIENCE

Advisor: Howard D. Mooers

2023

© 2023 Christa Wood

Acknowledgements

I would like to express my gratitude to those who have helped me along the way. First, my advisor, Howard Mooers who made an exception and took me on as graduate student when he was on the last sprint towards retirement. I appreciate the feedback, the assistance, and the conversations that invariably ended down a rabbit hole. I would like to thank my committee members, John Pastor and Phil Larson for their guidance along the way. I would also like to thank the numerous Professors in Heller Hall at the University of Minnesota, Duluth that I have taken classes from – you have all made Geology a joy to learn and study.

I would also like to thank my husband, Matt and my son, William, for their support, being willing to help around the house, and for gracefully bearing a little neglect. I want to thank my extended family and friends for being understanding when I had to turn down get-togethers and for listening to my grievances when I could show up. Finally, I would like to thank Molly, for her patience, her sound advice, and for reminding me of the important things.

Dedication

This thesis is dedicated to my aunt Linda, who left us too soon. You will never be far from my thoughts.

Abstract

Saprolite has been found in drill core across Minnesota and is overlain by Jurassic, Cretaceous, and glacial sediments. However, in the northeastern part of the State, which is characterized largely by glacially scoured bedrock, saprolite exposures can be found all along the North Shore of Lake Superior and inland where they are most well expressed in cliffside exposures and road cuts. This weathering residuum is typically associated with fault and fracture systems, and in some cases are preserved in the lee of competent rock types. Features of this saprolite include core stones, spherical weathering rinds, grus, and authigenic mineral formation along fractures.

The goals of this investigation were to inventory saprolite occurrences and characterize the geochemistry and clay mineralogy with emphasis on two sites where the remnant saprolite is well exposed in outcrops with a complete weathering sequence from least altered to highly weathered zones with authigenic mineral formation. Samples were submitted for major oxide and elemental analysis and mineral species were identified using powder X-Ray diffractometry with emphasis on clay mineralogy. The degree of weathering of samples was estimated using the Chemical Index of Alteration (CIA) (Nesbitt and Young, 1982) and the Chemical Index of Weathering (CIW). Isocon analysis is used to evaluate chemical losses and gains during weathering.

At the Crow Creek site, thirty meters of saprolite developed in mafic volcanic and intrusive rocks of the Midcontinent Rift are preserved. The unaltered diabase is composed of plagioclase, orthopyroxene, clinopyroxene, olivine, magnetite, and accessory minerals.The altered rock mineralogy is quartz, chlorite, talc, laumontite, prehnite, smectite, kaolinite, and illite.

The Silver Bay site exposes a deeply weathered pendant developed in granophyre. Unaltered granophyre is composed of K-feldspar, augite, apatite, plagioclase, and quartz. The highly altered weathering residuum has abundant iron oxide, calcite, smectite and Kaolinite.

The thickness, weathering progression, and authigenic mineral production suggest that these scattered exposures throughout NE Minnesota are the remnant of a once continuous pre-Pleistocene saprolite that covered the Canadian Shield. The age of the weathering is difficult to determine, but weathering on the Shield has been the dominant geological environment at least since the Late Proterozoic about 750 Ma ago, and likely much longer. Therefore, caution should be used when interpreting all of the saprolite in Minnesota as Mesozoic in age.

Table of Contents

List of Tables v
List of Figures vi
INTRODUCTION 1
BACKGROUND 4
Assembly of the North American Craton 4
Early Proterozoic (Paleoproterozoic) 5
The Huronian Basin 5
The Animikie Basin 6
Marquette Range 6
Animikie Group 6
Mid-Proterozoic 7
Late Proterozoic 8
Phanerozoic 9
Table 1. Summary of erosional unconformities 10
Pleistocene 10
Occurrence of Saprolite across Minnesota 12
METHODS 14
FIELD SITES 16
Crow Creek 16
Silver Bay 19
Spruce Road 21
McFarland Lake 22
Bald Eagle 23
Cascade River 23
Cores from DNR Core Library, Hibbing, MN 25
Characterization of weathering 26
Isocon Analysis 27
X-Ray Diffraction and Characterization of Weathering 27
RESULTS 28
Crow Creek Site 29
X-Ray Diffraction 33
Silver Bay 36
DISCUSSION 42
CONCLUSION 50
REFERENCES 53

List of Tables

Table 1 Summary of erosional unconformities……9

Table 2 List of identified saprolite outcrop exposures in NE Minnesota……..13

Table 3 Diabase sample descriptions with CIA and CIW calculations……...…..17

Table 4 Granophyre sample descriptions with CIA and CIW calculations……...…19

Table 5 List of major oxides and elements analyzed…….25

Table 6 Clay mineral low angle reflections with ethylene glycol and heat treatments……..27

Table 7 Oxides of selected Crow Creek samples……...…29

Table 8 Oxides of selected Silver Bay samples…….36

List of Figures

Figure 1. Location of saprolite exposures identified by this study. 1
Figure 2. Illustrations of core stones, spherical weathering rinds, grus, and authigenic mineral formation along fractures. 2
Figure 3. Occurrence of saprolite in the subsurface from drill core logs. 13
Figure 4. Sampling locations at Crow Creek site. 16
Figure 5. Sample location of CC-3. 16
Figure 6. Sample locations of CC-8, CC-9, CC-10, and CC-13. 17
Figure 7. C-1 sampled white grains occurring on outcrop. Grains ranged from translucent to opaque and were 1/2" or smaller in size. 17
Figure 8. Sampling locations at the Silver Bay site. Yellow circles are samples that were chosen for geochemical analysis. Sample 13 (orange) was collected on a secondary visit for XRD verification of clays. 19
Figure 9. Weathered outcrop from which a drill core, weathering rind, and grus were sampled at Spruce Road. 21
Figure 10. Core stone with weathering rind at McFarland Lake. 22
Figure 11. Bald Eagle outcrop. 23
Figure 12. Core stone, weathering rind, and interstitial material sampled at Cascade River. 24
Figure 13. Drill core from the Thistledew Lake Sequence. 25
Figure 14. Outcrop site CIA and CIW comparisons. The chart illustrates that the more mafic sites follow a similar weathering indices trendline, while the Silver Bay granophyre is clustered above the trendline. 29
Figure 15. Isocons of the major oxides at Crow Creek. 32
Figure 16. Diffractogram of the selected fine sediment samples from Crow Creek. 33
Figure 17. Diffractogram of prehnite grain from Crow Creek. 34
Figure 18. Diffractogram of lizardite (serpentine) and talc. 34
Figure 19. Air-dried, glycolated, and heated diffractogram patterns of Crow Creek vein fill. 35
Figure 20. Isocons of the oxides from Silver Bay. 39
Figure 21. X-Ray Diffraction of granophyre powder samples. 40
Figure 22. XRD patterns of feldspars, augite, apatite, calcite, quartz, Fe-oxides, Fe-Ti oxides, and kaolinite. 41
Figure 23. Air-dried, glycolated, and heated diffractogram patterns of Silver Bay granophyre. 42
Figure 24. Hoinkes et al. (2005) illustrated incipient metamorphism diagram. 46
Figure 25. Temperature-Pressure diagrams illustrating thermal gradients of zeolites from Kuethe, 2016. 46
Figure 26. Temperature-Pressure diagrams illustrating thermal gradients of prehnite from Kuethe, 2016 47

INTRODUCTION

The landscape of northeastern Minnesota has a well-documented history of repeated Pleistocene glaciations (Mooers and Lehr, 1997; Clark and Pollard, 1998; Larson, 2008; Dyess and Hansen, 2014; Krabbendam and Bradwell, 2014). In general, the terrain is characterized by Precambrian ice-scoured igneous and metamorphic bedrock a billion or more years old overlain by a veneer of glacial sediment of varying thickness deposited in the past few tens of thousands of years. However, local outcrops throughout the region contain areas of bedrock deeply weathered into saprolites that are sporadically preserved. These saprolites can be found exposed all along the North Shore and inland where they are most well expressed in cliffside exposures and road cuts.

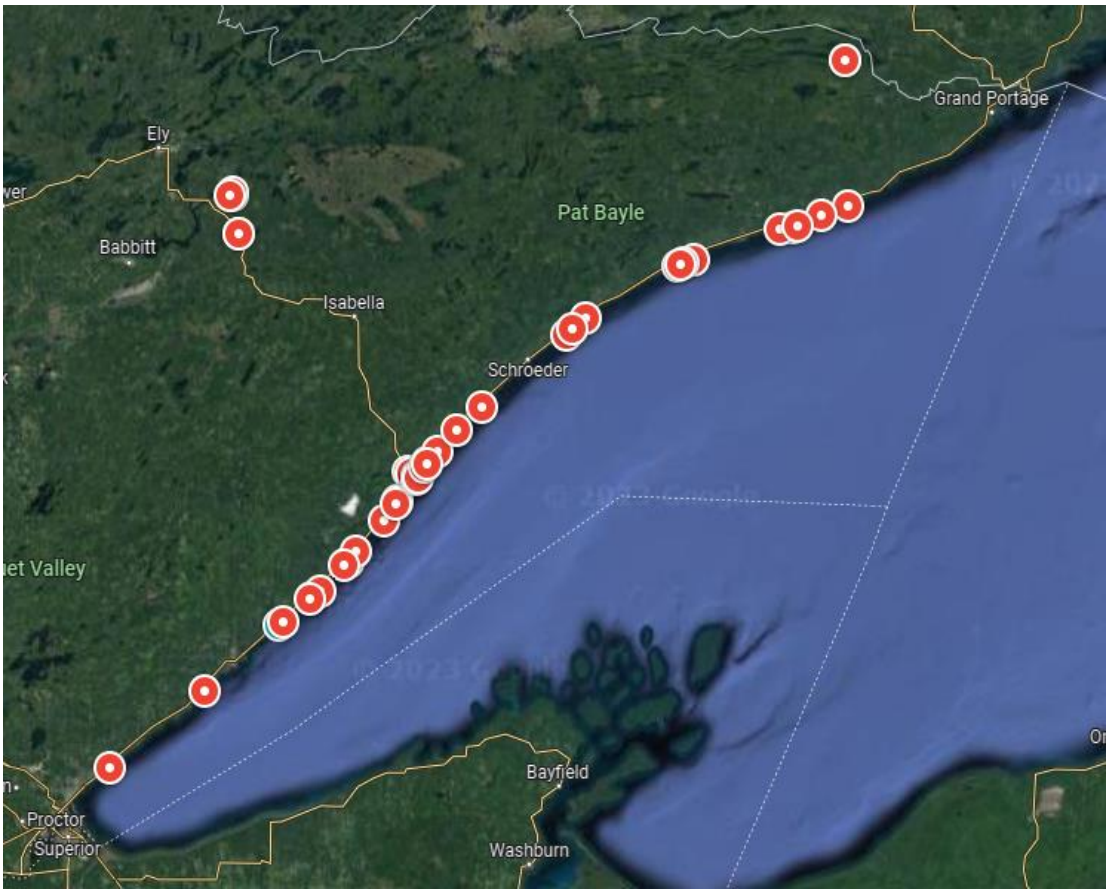

Figure 1. Location of saprolite exposures identified by this study.

This weathering residuum is typically associated with fault and fracture systems, and in some cases are preserved in the lee of competent rock types. Features of this saprolite include core stones, spherical weathering rinds, grus, and authigenic mineral formation along fractures. A few of these exposures have been documented to be rather thick, in some cases tens of meters.

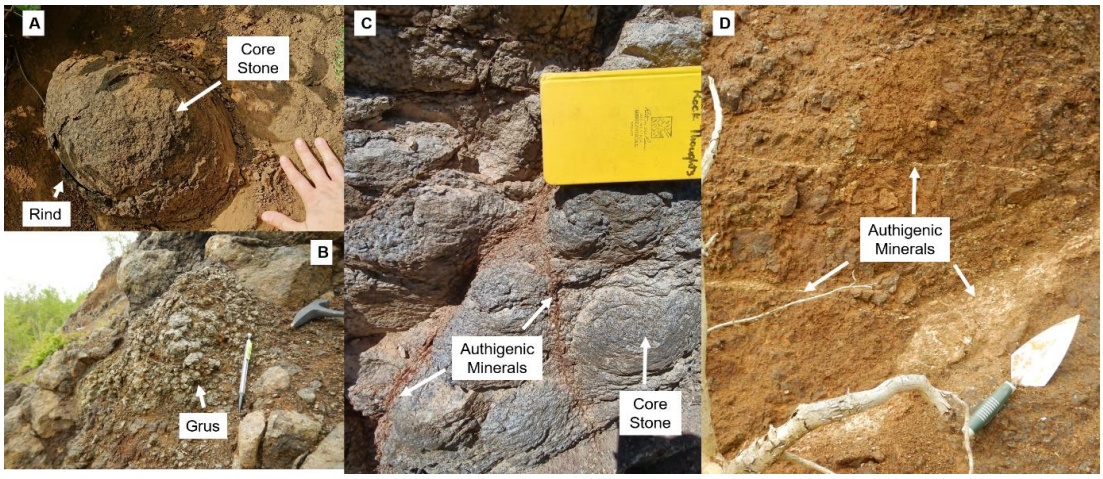

Figure 2. Illustrations of core stones, spherical weathering rinds, grus, and authigenic mineral formation along fractures.

For example, near Silver Bay, there is a weathered pendant within granophyre, likely representing deep weathering along a fracture. This site has highly weathered components and incipient core stone formation with developing weathering rinds. One of the thickest and most extensive occurrences of saprolite exposed along the North Shore of Lake Superior is near Crow Creek. Here, the exposure is a road cut through Lafayette Bluff, exposing a highly weathered diabase sill where the saprolite is approximately thirty meters thick.

These weathered rocks have received very little attention in literature. Winchell's (1900) report of the geology of Minnesota mentioned occasional weathering observed throughout the state, but was restricted to basic field observations. Upham (1904) briefly described the occurrence of weathered boulders that had been glacially transported in the tills of Butte, Montana, surmising that the core stones were features of a widespread saprolite stripped by glaciation. Goldich (1938) was the first to conduct an in-depth study on rock weathering in the state in the Minnesota River Valley and at

the aforementioned Crow Creek diabase, but was limited by the technology of the time, which did not allow the identification of specific clay mineral species.

Some workers have suggested that these exposures of weathering residuum are postglacial in age, that is, Late Wisconsinan and Holocene (John C. Green, personal communication, January 2021). Others have considered the weathering of Minnesota bedrock to be Jurassic - Cretaceous in age consistent with the warmer climate that existed at the time (Parham, 1970; Setterholm and Morey, 1989; Roy et al., 2004; Medaris et al., 2022). The thickness, weathering progression, and authigenic mineral production suggest that these scattered exposures throughout NE Minnesota may be the remnant of a once continuous preglacial saprolite that covered the Canadian Shield.

It is widely accepted that prior to glaciation North America was covered by an extensive saprolite (Chalmers, 1898; Clark and Pollard 1998; Bouchard and Jolicoeur, 2000; O'Beirne-Ryan and Zentilli, 2003; Jansson & Lidmar-Bergström, 2004; Zauyah et al., 2010). In Minnesota, well-developed saprolite is commonly preserved throughout the state in boreholes at the base of the Pleistocene sequence. Pre Illinoisan tills in Kansas and Nebraska contain significant components of kaolinite, suggested to have been incorporated into early Pleistocene tills from saprolite erosion by ice sheets (Hallberg, 1980). Clark and Pollard (1998) theorized frequent (41 kyr), low volume glaciations prior to the mid Pleistocene transition occurred over soft-sediment beds of saprolite, and the mid Pleistocene transition was the result of the stripping of the saprolite switching basal ice conditions to a hard bed of Canadian Shield bedrock, which favored 100 kyr frequency, high volume ice sheets.

The goals of this investigation are to inventory saprolite occurrences and characterize the geochemistry and clay mineralogy with emphasis on two sites where the remnant saprolite is well exposed in outcrops with a complete weathering sequence from least altered to authigenic mineral formation. The two sites are from the Mid-Continent rift volcanics, in particular a mafic diabase sill at Crow Creek between 1098.5 and 1096.1 Ma in age (Paces and Miller, 1993; Davis and Green, 1997;

Fairchild et al., 2017) and a granophyre intrusion north of Silver Bay which was dated at 1094 Ma (Juda, 2006). Analyses from several other sites are used to highlight the nature and extent of the saprolite and as supporting documentation.

BACKGROUND

The North American craton is the world's largest preserved craton (Percival et al., 2012; Jaupart et al., 2014), and since its formation is considered relatively undisturbed (Card and Ciesielski, 1986). However, the stratigraphy of the Superior province is marked by a number of unconformities suggesting a complicated erosional history (Sims, 1972; Erikson and Condie, 2014).

Assembly of the North American Craton

Craton formation is achieved through multiple processes of the separation of continental crust from the mantle and the amalgamation of crustal blocks (Jaupart et al., 2014; Card, 1990). The North American craton is Archean in age, with the Superior Province (3.1 Ga - 2.6 Ga) being inferred as the continental nucleus (Hoffman, 2007; Card, 1990, Percival, 2007). The oldest regions of the craton are the Northern Superior superterrane (3.7 Ga) and Minnesota River Valley terrane (3.6 Ga) in the south, which are both considered to be amalgamated terranes existing prior to assembly of the craton at 2.72 Ga and 2.68 Ga (Percival, 2007). The accretion of the craton is the product of five major orogenies: Northern Superior Orogeny (2.72 Ga), Uchian Orogeny (2.72 - 2.7 Ga), Central Superior Orogeny (2.7 Ga), Shebandowanian Orogeny (2.69 Ga), and the Minnesota Orogeny (2.68 Ga) (Percival et al., 2012). The youngest regions of the craton are dated at 2.8 Ga to 2.7 Ga and include ocean floor, island arcs, and continental arcs (Bickford et al., 2007, Percival et al., 2012). The final assemblage consisted of terranes of granite-greenstone and gneiss (Nelson, 1998; Percival et al., 2012, Lodge et al., 2013).

The formation of the supercontinent Kenorland starting at 2.75 Ga produced the Algoman (Kenoran) orogeny, which was the last major event in the late Archean (Lepp and Goldich, 1964; Sims 1972; Card, 1990). This mountain building event was a collision between the Superior Province and the Minnesota River Valley terrane and is associated with granitic plutons and greenschist metamorphism (Vervoort, 1987). Davidson (1980) studied the Saganaga tonalite batholith emplacement at 2.7 Ga in the southwest of the province, describing it as undergoing rapid unroofing and deformation. A subaerial

weathering profile quickly developed on the Saganaga tonalite associated with uplift and unroofing (Lodge et al., 2013) and high pCO_2 in the paleoatmosphere (Dreise et al. 2011), and is unconformably overlain by the Ogishkemuncie sequence (2.68 Ga) (Lodge et al., 2013). Between 2.73 Ga and 2.67 Ga, four cycles of sediments were deposited in the Abitibi Greenstone belt in Quebec, Canada, in basins that younged southward and include deep-water facies (cycles 1 and 3) including Algoma-type iron formations and shallow marine sediments (cycle 2 and 4) that are marked by a number of unconformities and deformations related to tectonic and magmatic activity (Mueller and Donaldson, 1992; Hoffman, 2007; Thompson, 2015; Taner and Chemam, 2015).

Early Proterozoic (Paleoproterozoic)

Ojakangas et al. (2001b) described the Superior Province as a peneplain at the Archean-Proterozoic transition at 2.5 Ga. By 2.45 Ga Kenorland began to rift apart, which has been attributed in part to the Matachewan plume. The result of the early rifting was the Matachewan large igneous province and dike swarms south of the Huronian basin (Ciborowski et al. 2015; Young, 2015). The Kapuskasing uplift at 2.1 Ga emplaced diabase dike swarms associated with intracratonic thickening which interrupted the continuity of the Matachewan dike swarms (Halls and Zhang, 1998; Percival et al., 2012; Lin et al, 2013). Halls et al. (2008) studied the 2.07 Ga Marathon large igneous province northeast of Lake Superior that emplaced the associated Kapuskasing, Marathon, and Fort Frances dike swarms to the west of Lake Superior, all of which are thought to be genetically related to the same plume. Formations associated with early rifting include the Livingstone Creek Formation sandstones and the Thessalon Formation volcanics (Young et al., 2001; Young, 2015).

The Huronian Basin

Young (2019) described the Huronian group sediments (2.5 - 2.2 Ga) that were unconformably deposited in the Huronian Basin on Archean basement rocks in the central south of the Superior Province, extending from the modern day eastern shore of Lake Superior to the Ontario-Quebec border. The Huronian Supergroup contains the earliest global evidence of glaciation in the Ramsay Lake Formation with at least three separate glacial events recorded in its stratigraphy (Ramsay Lake, Bruce, and Gowganda)

interspaced by periods of greenhouse conditions (Fedo et al., 1997; Craddock et al., 2013; Young, 2014; Bekker, 2015; Young, 2019). Weathering horizons have been observed on the glacial deposits and overlying units. The Lorrain Formation (2.3 Ga) in particular preserves an abrupt post-glacial extreme weathering event associated with a hot climate and high concentrations of atmospheric CO_2 related to build-up during the previous glacial period and continental rifting volcanism (Rainbird et al., 1990; Young, 2013; Bekker, 2015; Young, 2019). The Huronian Supergroup also contains Superior-type banded iron-formations which were likely sourced from an intensely weathered and eroded Archean Superior Province based on mass-balance relationships between the sediments and the source composition (Nesbitt and Young, 1982; Rainbird et al., 1990; Fedo et al, 1997, Young, 2002; Eriksson and Condie, 2014; Young, 2019). The Huronian Supergroup contains a stratigraphic gap from 2.2 Ga to 1.85 Ga during which the continent became a peneplain and the Whitewater Group turbidites were unconformably deposited on top of the Huronian rocks (Robertson and Card, 1972; Young 2013; Young 2019).

The Animikie Basin

Marquette Range

In the south-central of the superior province of Michigan and Wisconsin, the Marquette Range Supergroup (2.5 Ga - 2.11 Ga) deposited sediments unconformably on the Archean basement in the eastern branch of the Animikie basin (Jirsa et al., 2004; Vallini et al., 2006; Sekine et al. 2007; Cannon et al., 2008). The Marquette Range Menominee Group contains Superior-type banded iron formation and granular iron formation (Klein, 2005; Pietrzak-Renaud, 2013). The iron ranges within the Marquette Range include the Gogebic, Marquette, Menominee, and Iron River-Crystal Falls (Cannon et al., 2008).

Animikie Group

The western Animikie Basin hosts the Animikie Group (2.5 Ga - 1.8 Ga) deposited as sediment in near-shore and marine waters which extends from South-central Minnesota to Thunder Bay, Ontario (Ojakangas et al., 2001b; Young, 2002; Jirsa et al., 2004; Craddock et al, 2013; Young 2015). Ojakangas et al. (2011) described the basal layer of the Animikie group, the Pokegama Formation, as unconformably overlying the Archean granitic basement. Purucker (1983) thought the sediments were sourced from

regolith that developed on rocks from the Precambrian to the Devonian. The group contains Superior-type banded iron formations in the Gunflint, Mesabi, Vermillion, Gogebic, and Cuyuna Ranges (Morey, 1978; Purucker, 1983). The Fern Creek Formation (~2.3 Ga) of both the eastern and western Animikie basin is considered the equivalent of the Gowganda of the Huronian Supergroup and contains an ancient weathering profile on glaciogenic diamictites (Ojakangas et al., 2001b; Young 2019). The Sturgeon and Mesnard Quartzites which correlate to the Lorrain Formation (2.3 Ga) of the Huronian Group contain a weathering profile (Ojakangas et al., 2001b; Young 2019). Young (2015) said the Huronian, Marquette Range, and Animikie Groups all record a stratigraphic gap from 2.2 Ga to 1.85 Ga, which he suggested was related to a prolonged two-stage break up of Kenorland. The end of the stratigraphic gap coincides with the Sudbury impact at 1.85 Ga, which is associated with thick carbon deposits (Young, 2002; Mossman et al., 2003). The end of the iron deposit formation at 1.8 Ga is thought to be related to changing oceanic conditions. Young (2002) suggested there might have been a decrease in oceanic hydrothermal activity and iron production related to a cooling of the earth's interior. Poulton et al. (2010) postulated that increasing euxinic oceanic conditions from 1.8 Ga to 0.58 Ga lead to the consumption of iron in pyrite formation and was responsible for the end of the iron formations.

Mid-Proterozoic

The Mid-Proterozoic was marked by further amalgamation of the craton and mountain building events. At 1.9 - 1.8 Ga the Trans-Hudson and Penokean orogenies were active to the western and southern margins of the Superior Province, respectively (Lepp and Goldich, 1964; Weller and St-Onge, 2017). The Trans-Hudson orogeny was formed by the collision of the Superior and Hearne cratons and is best associated with the Kisseynew metasedimentary gneiss belt (Ansdel et al., 1995, Machado et al., 2000). The collision of the Superior craton and the Pembine-Wausau Terrane (1.88 Ga) and later the Marshfield craton (1.85 Ga) created the Penokean northward thrust belt that deformed the Huron, Marquette, and Animikie groups (Schulz and Cannon, 2007; Craddock et al., 2018). From 1.8 Ga - 1.6 Ga the southern margin of the Superior Province was subject to post-Penokean intrusive granites thought to be related to extension (1.7 Ga) (Ojakangas et al., 2001b; Sekine et al. 2007) as well as metamorphic and deformation overprinting events that some have suggested may be related to the Yavapai orogeny and

to a lesser extent, the Mazatzal orogeny, that are more commonly associated with the American southwest (Schulz and Cannon, 2007; Holm et al., 2020).

Late Proterozoic

The craton remained relatively quiet until Mid-continent rifting in the late Proterozoic (*ca.* 1.1 Ga) produced the North Shore Volcanic Group and the Duluth Complex layered intrusions (Sims, 1972; Ojakangas et al., 2001a). The Mid-Continent Rift System was active for approximately 25 million years and was a multi-stage event resulting in volcanic and sedimentary clastic rocks filling the rift (Percival et al., 2012; Miller et al., 2013; Fairchild et al., 2017). The rift was approximately 20 km wide and trended 2000-2500 km from Kansas to southeast Michigan, although exposure is limited to the Lake Superior region (Ojakangas et al., 2001a; Percival et al., 2012; Hinze and Chandler, 2020). Paleomagnetic data suggest the rocks were deposited at tropical to subtropical latitudes during a period of magnetic polarity reversal (Turek and Robinson, 1984; Ojakangas et al., 2001a). Cannon (1992) estimated the original volume of erupted rock to be at least 2 million km^3 in thicknesses of 20 km or greater with approximately 0.5 million km^3 having been eroded since. Green (1989) described the North Shore Volcanic Group as high-volume basalt and basaltic-andesite, moderate to small volume basalts, and small to large flow rhyolites and icelandite. The North Shore Volcanic Group "roof" the Duluth Complex intrusions. The Duluth Complex emplaced over 4.4 billion metric tons of primarily mafic magma along the shore of Lake Superior from Duluth to Pigeon Point in Minnesota, and is enriched in Cu-Ni-PGE sulfides (Fix, 2015). It consisted of anorthositic, troctolitic, gabbroic, and some granitic layered mafic intrusions (Miller and Ripley, 1996; Ojakangas et al., 2001a; Miller et al., 2013). Glacial sediment cover has made preserved weathering rare on the surface. Drill cores of the subsurface show that oxidation is not extensive (Fix, 2015).

The Proterozoic Grenville orogeny (1.1 Ga) to what is now the east is postulated to be responsible for the failure of the Midcontinent Rift System (Lepp and Goldich, 1964; Ojakangas et al., 2001a; Percival et al., 2012). The Grenville orogeny was a rapid response to the formation of Rodinia as the paleo-continents of Laurentia and Baltica collided with Amazonia (Slagstad et al., 2017; Swanson-Hysell et al., 2019; Johnson et al., 2020). Hinze and Chandler (2020) interpreted the Grenville front location as

extending from northern Alabama up through Newfoundland, Canada and intersecting the eastern arm of the Mid-Continent Rift System in present-day southeast Michigan. Karlstrom et al. (1999) described emplacement of northeast trending mafic dikes associated with intracratonic extension from the upper Northwest Territory to southern Ontario as occurring at the same time as the Grenville orogeny.

By the end of the Proterozoic, the activity of the craton's interior slowed and much of the geologic processes ongoing at the time were surficial in nature. Core samples of basement rocks from southern Ontario, Canada, were reported to have 3 cm to 3 m of regolith suggesting weathering and erosion of the province occurred from 950 Ma to 600 Ma, resulting in peneplaining of the craton (Robertson and Card, 1972; Turek and Robinson, 1984). Farley and McKeon (2015) dated hematite enrichment from supergene weathering in the Gogebic iron range that occurred in two different events at ~772 Ma and 453 Ma. It is likely the dominant geologic processes at the time were weathering and erosion.

Phanerozoic

Rodinia rifted apart between 750 Ma and 550 Ma among intermittent glaciation and deposition of Rapitan type iron formations recorded in the Rapitan Group of Yukon, Canada (Morris, 1977; Karlstrom et al., 1999; Eyles and Januszczak 2004; Li et al., 2013; Rooney et al., 2013; Williams et al., 2016). After the rifting of Rodinia, the interior of the craton remained tectonically stable with tectonic activity relegated primarily to the continental margins.

From the early Paleozoic to the Cenozoic, six cratonic sequences of marine transgressions and regressions deposited sediments across most of the craton with the greatest coverage during the Silurian (Tippecanoe Sequence) advance (Sloss, 1988; Levin, 2003; Cocks and Torsvik, 2011; Karlstrom et al., 2018). A limited sequence of sediments were deposited and preserved in SE Minnesota from these sequences with primarily sand during the Cambrian, Ordovician carbonates, and Devonian carbonates from the Hollandale Embayment (Runkel et al., 2007). The NW corner recorded Ordovician carbonates and limited buried Jurassic mudstones. The last major transgression on the western half of Minnesota occurred during the Cretaceous, and was responsible for the deposition of siltstones, shale, and sandstones (Sloan, 1964). The last cratonic sequence is associated with a warm subtropical climate and credited with

intense chemical weathering by the later Cretaceous (Patterson and Boerboom, 2017; Medaris et al., 2022).

Table 1. Summary of erosional unconformities

Unconformity	Event	Age	Reference
Saganage Tonalite	Weathering	2.7 Ga emplacement	Davidson, 1980, Dreise et al., 2011; Lodge et al., 2013
Abitibi Basin -Fivemile Lake Sequence	Weathering	2.73-2.67 Ga	Hoffman, 2007
Peneplain	Erosion	2.5 Ga	Ojakangas et al., 2001b
Huronian Basin -Ramsay Lake, Bruce, and Gowganda glacial formations -Lorrain Formation -Superior-type BIF	Weathering Weathering Weathered sediments	2.5 - 2.2 Ga 2.3 Ga	Rainbird et al., 1990; Fedo et al., 1997; Craddock et al., 2013; Young, 2013; Young, 2014; Bekker, 2015; Young, 2019
Animikie Basin – Marquette Range -Superior-type BIF -Fern Creek Fm (Gowganda Fm equivalent) -Sturgeon and Mesnard Quartzites (Lorrain Fm equivalent)	Weathered sediments Weathering Weathering	2.5 – 2.11 Ga ~2.3 Ga 2.3 Ga	Ojakangas et al., 2001b; Jirsa et al., 2004; Klein, 2005; Vallini et al., 2006; Sekine et al. 2007; Cannon et al., 2008; Pietrzak-Renaud, 2013; Young 2019
Animikie Basin – Animikie Group -Superior-type BIF -Fern Creek Fm (Gowganda Fm equivalent) -Sturgeon and Mesnard Quartzites (Lorrain Fm equivalent)	Weathered sediments Weathering Weathering	2.5-1.8 Ga ~2.3 Ga 2.3 Ga	Purucker, 1983; Ojakangas et al., 2001b; Jirsa et al., 2004; Ojakangas et al., 2011; Young, 2019
Peneplain	Erosion	1.85 Ga	Robertson and Card, 1972; Young 2013; Young 2019
Southern Ontario - Basement Core Samples	Weathering	950 Ma – 600 Ma	Turek and Robinson, 1984
Gogebic Range	Weathering	772 Ma, 453 Ma	Farley and McKeon, 2015
Cretaceous warm climate	Weathering	144 Ma – 66 Ma	Patterson and Boerboom, 2017; Medaris et al., 2022
Pleistocene Glaciation	Erosion	2.58 Ma – 11,700 a	Gibbard et al., 2010; Walker, 2019

Pleistocene

By the early Pleistocene, the surface of the craton was thought to be the exposed Archean basement rocks that were covered in a weathering residuum from intense Proterozoic weathering. Patterson and Boerboom (1999) suggest the entire state of Minnesota had an average of 30 m of weathered bedrock by the end of the Cretaceous. Roy et al. (2004) asserted the bedrock regolith in the Minnesota River valley was pre-Cretaceous and averaged to depths of 45-60 m, but could exceed depths of 90 m. Rutter (1980) using Strakhov's (1967) calculations for weathering granitic rocks suggested any significant weathering would have occurred prior to the Pleistocene as interglacial periods would not permit enough time to significantly alter the bedrock. Medaris et al. (2022) suggested much of the weathering would have occurred along various unconformities in Phanerozoic rocks despite lower CO_2 levels, potentially due to the arrival of land plants capable of producing organic acids during the Cambrian.

The Pleistocene was marked by a return of episodic glaciation to the craton. It has been suggested that glaciers are highly efficient vehicles of erosion. However, Pleistocene ice sheets have been hypothesized to be limited in their ability to remove competent bedrock both on the Canadian and Fennoscandian (Baltic) shields (Rutter, 1980; Lidmar-Bergstrom, 1995, 1997; Olvmo et al., 2005; Clark and Pollard, 1998; Patterson and Boerboom, 1999; Hall et al., 2013). Flint (1971) described the exposed, post-glaciated surfaces of the Canadian Shield basement as having "...almost the same appearance and relief as the surface still unconformably covered by Ordovician strata. Evidently, glaciation failed to modify more than the details of the relief." Early Pleistocene marine isotope records suggest the volume of the ice sheets were relatively small and occurring in 41,000 year Milankovitch glacial cycles (Roy et al., 2004). At this time, the ice in North America was also the most laterally extensive, advancing as far as the southern reaches of the Midwest (Clark and Pollard, 1998; Roy et al., 2004).

The Mid-Pleistocene Transition at about 900 ka was characterized by a change in glaciation frequency to 100,000 year cycles, with much greater ice volume and has been interpreted by Clark and Pollard (1998) that the change was related to the widespread stripping of the regolith. Prior to the mid-Pleistocene, the weathering horizon had yet to be removed and glacial soft-bed conditions allowed for low-amplitude, but greater lateral advances of the Laurentide ice sheet. After the transition, it is thought that the weathered horizon had been largely removed leaving a consolidated bedrock, which supported a higher

basal shear stress, higher-amplitude, lower frequency, and therefore greater ice volume (Clark and Pollard, 1998; Larson, 2008).

Prior to Wisconsinan glaciation, bed conditions on the Canadian Shield are unknown, though it is assumed that there was a thin layer of glacial sediment present. Larson (2008) suggested that following the removal of the regolith, the unconsolidated till left behind from previous glaciations and the transport of sediments from the reservoir in the Hudson Bay basin and lowlands onto the Precambrian shield allowed similar soft-bed basal conditions on a localized scale. The relatively thin till and basin sediments would be subject to rapid glacial erosion as the ice sheet grew and the zone of maximum velocity moves out from Hudson Bay resulting in a return to hard-bed conditions and a thick ice sheet.

Occurrence of Saprolite across Minnesota

At present time, preserved saprolites are found in drill cores and isolated surface exposures along the shore of Lake Superior in northeast Minnesota.

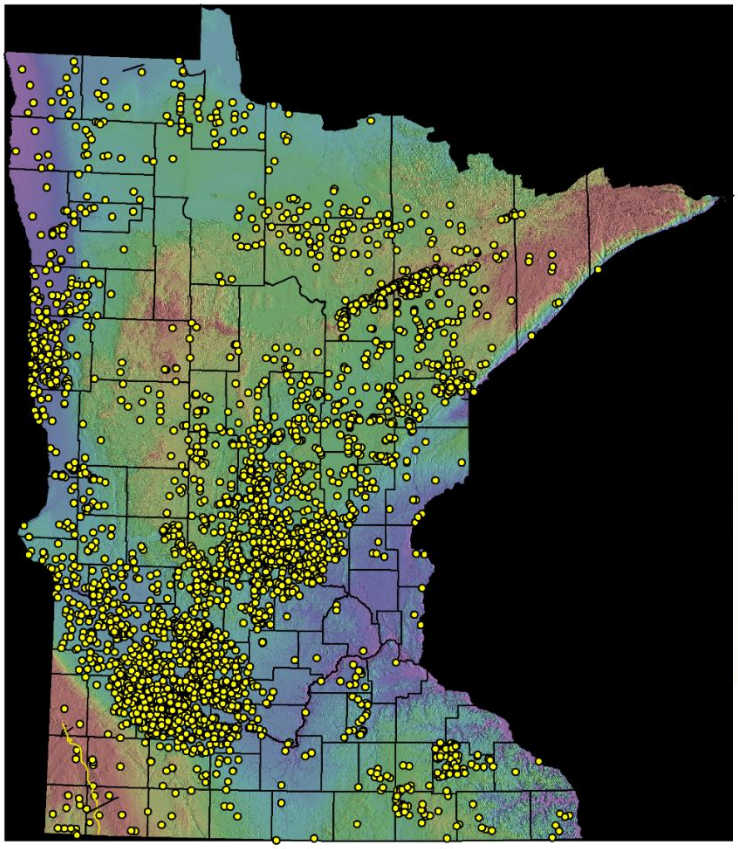

Figure 3. Occurrence of saprolite in the subsurface from drill core logs (Minnesota Well Index, 2023).

Saprolite has been found in drill core across the state (Figure 3) and is overlain by Jurassic sediments in extreme NW Minnesota, Cretaceous sediments throughout much of the State, and glacial sediments. The age of the weathering is poorly constrained, but simply by stratigraphic position is early or pre Cretaceous, early or pre Jurassic. Recall that Farley and McKeon (2015) conducted helium dating on ore of the Gogebic Range, which returned dates off 772 ± 41 Ma for two samples and 453 ± 14 Ma for a third sample, suggesting that weathering may have either been continuous or episodic at least since the late Proterozoic. In addition, there are weathered horizons within the Midcontinent Rift flows that have been

subsequently buried by later lava flows, and therefore that weathering dates to the time of the Midcontinent Rift (Seifert and Anderson, 1996; Mitchell and Sheldon 2009).

METHODS

Saprolite exposures in road cuts along the northeastern shore of Lake Superior from Duluth to Grand Marais were inventoried (Table 2, Figure 1). Additional weathering profiles were examined in drill core based on descriptions of saprolite in boreholes. Sample sites were selected based upon known outcrop locations, accessibility, and extent of weathering profile. Samples were collected from outcrops, and drill core archived at the Department of Natural Resources Core Repository in Hibbing, MN.

Table 2. List of identified saprolite outcrop exposures in NE Minnesota.

Site	Lat	Long	Classification	Analyses
Crow Creek	47.098053	-91.550042	Diabase	*MEG, **XRD
Silver Bay	47.308439	-91.24025	Granophyre	*MEG, **XRD
McFarland Lake	48.060897	-90.068733	Gabbro	*MEG, **XRD
Spruce Road	47.831353	-91.679328	Gabbro	*MEG, **XRD
Bald Eagle Intrusion	47.742908	-91.641614	Gabbro	*MEG, **XRD
Cascade River	46.8485998	-91.9942278	Basaltic Andesite	*MEG, **XRD
Unnamed Location	47.7115235	-90.5061845		
Unnamed Location	47.15498	-91.44452		
Unnamed Location	47.3084214	-91.2401965		
Unnamed Location	47.765628	-91.6570144		
Unnamed Location	47.8312939	-91.6792828		
Unnamed Location	47.8355287	-91.6735402		
Unnamed Location	46.8485998	-91.9942278		
Unnamed Location	46.982212	-91.745635		
Unnamed Location	47.1990558	-91.3810396		
Unnamed Location	47.2753495	-91.2750565		
Unnamed Location	47.2216007	-91.3501268		
Unnamed Location	47.1445399	-91.4656683		
Unnamed Location	47.2043663	-91.3676336		
Unnamed Location	47.350064	-91.1899382		
Unnamed Location	47.3490175	-91.1897981		

Unnamed Location	47.3522003	-91.1913819		
Unnamed Location	47.3567653	-91.2072824		
Unnamed Location	47.358982	-91.2124165		
Unnamed Location	47.7748023	-90.2407594		
Unnamed Location	47.7764352	-90.203005		
Unnamed Location	47.7787262	-90.1913575		
Unnamed Location	47.797283	-90.128489		
Unnamed Location	47.8127936	-90.0614394		
Unnamed Location	47.3738709	-91.1650426		
Unnamed Location	47.7131353	-90.4985838		
Unnamed Location	47.60336	-90.78254		
Unnamed Location	47.594602	-90.7965916		
Unnamed Location	47.4312141	-91.0863651		
Unnamed Location	47.39445	-91.13647		
Unnamed Location	47.3747159	-91.1643624		
Unnamed Location	47.3680911	-91.1706756		
Unnamed Location	47.3491129	-91.1850801		
Unnamed Location	47.34676	-91.18872		
Unnamed Location	48.0609662	-90.0688617		
Unnamed Location	47.4690666	-91.0199448		
Unnamed Location	47.6217894	-90.7462891		
Unnamed Location	47.71176	-90.5062		
Unnamed Location	47.7151972	-90.492126		
Unnamed Location	47.722504	-90.462504		
Unnamed Location	47.304488	-91.245017		
Unnamed Location	47.102	-91.53997		
Unnamed Location	47.1420921	-91.4703628		
Unnamed Location	47.10193	-91.54005		

*MEG – Multi-element geochemistry
**XRD – X-ray diffraction

FIELD SITES

Crow Creek

Figure 4. Sampling locations at Crow Creek site.

Figure 5. Sample location of CC-3.

Figure 6. Sample locations of CC-8, CC-9, CC-10, and CC-13.

CC-11 and CC-12 do not have a closer view due to precarious conditions for photography.

Figure 7. C-1 sampled white grains occurring on outcrop. Grains ranged from translucent to opaque and were 1/2" or smaller in size.

Table 3. Diabase sample descriptions with CIA and CIW calculations; see Equations 1 and 2 below.

Sample	Description	CIA	CIW
CC-1	white fibrous grains	30.5	30.6
CC-2	Highly grussified material	45.6	45.8
CC-3	core stone	46.1	46.4
CC-8	vein material	41.6	42.6
CC-9	Highly grussified material next to CC-8 vein on right	47.2	47.4
CC-10	Highly grussified material next to CC-8 vein on left	45.0	45.1
CC-11	core stone and grus	46.5	46.8
CC-12	vein material	50.2	50.5
CC-13	vein material	44.2	44.5
CC-14	vein material	35.5	35.9

The Crow Creek saprolite exposure is on highway 61 about 5 miles north of Two Harbors, Minnesota, along the western shoreline of Lake Superior. It is visible from the road roughly 300 feet north of Layfayette Bluff Tunnel on Layfayette Bluff. The site is part of the 600-foot-thick Layette Bluff porphyritic diabase sill that intruded Keweenawan Supergroup. Pope (1976) studied the unweathered main phase and used petrographic thin sections to describe the sill mineralogy. He described the unweathered diabase containing plagioclase phenocrysts, high-alumina olivine, pyroxenes, opaques, apatite, and amygdaloidal minerals with the sill itself being slightly Fe-enriched. Goldich (1938) conducted geochemistry on the site and concluded that there was remarkable chemical similarity between the unweathered and weathered mineralogy and limited significant differences to moisture content and proportions of ferrous and ferric oxides.

The sampling location was approximately seventy feet up the side of the bluff. The exposure is approximately 160 feet wide and varies from roughly 40 feet to 80 feet in height. Outcrops are sporadic among a cover of red-brown sand-sized material. The diabase is porphyritic and weathers to dark red-brown crumbly cobbles to a coarse red-brown sand. Weathering stages present included incipient core stones, grus, and presumed authigenic minerals. The site was cross-cut with thin veins of a pink material at various orientations. Fifteen samples were collected from the locations shown in Figures 4, 5, 6, and 7 and they are tabulated in Table 3. An effort was made to collect samples that represent a range of

weathering. Samples CC-11 and YY were corestones, 20 and 40 cm in diameter, respectively; these were chosen to represent the least altered components of the exposure. Progressively greater degrees of decomposition were sampled. Samples CC-3 and CC-11 represent least weathered core stones. Samples CC-8, CC-12, and CC-14 are vein fills, potentially representing the most altered or authigenic components of the weathering system.

Silver Bay

Figure 8. Sampling locations at the Silver Bay site. Yellow circles are samples that were chosen for geochemical analysis. Sample 13 (orange) was collected on a secondary visit for XRD verification of clays.

Table 4. Granophyre sample descriptions with CIA and CIW calculations; see Equations 1 and 2.

Sample	Description	CIA	CIW
G-1	Alt rock	55.7	86.3
G-2	Core stone with calcite	60.3	85.0
G-3	Grussy sand (red-brown)	63.7	85.0
G-4	Grus - various sizes	59.6	77.0
G-7	Sandy Grus (Vein)	57.2	83.3
G-12	Unalt rock	56.5	67.4

The Silver Bay site is hosted within the Beaver Bay Complex, which is composed of multiple hypabyssal intrusions of gabbro and diorite with a single red-rock granophyric phase, the Finland granite.

The Silver Bay intrusions are the youngest suite of the southern Beaver Bay Complex (Miller and Chandler, 1997). Gehman (1957) first noted a granodiorite intrusion, but did not conduct an in-depth study. Miller and Chandler (1997) categorized the granodiorite as a leucogranite and suggested that it possibly formed from the localized melting of felsic footwall rocks.

Located along highway 61 on Rieder Memorial Drive, the saprolite is a weathering pendent formed within a presumed fracture of a massive medium-grained, equigranular granodiorite. Hand samples contain quartz, potassium feldspar, plagioclase feldspar, and augite. Granodiorites of the Beaver Bay Complex were previously observed by Gehman (1957) who noted that the dikes were abundant and all contained potassium feldspar with the reddish coloration from hematite. He observed a diversity of textures, leading him to conclude that there were multiple periods of intrusions and postulated the dike may have no genetic relations to the Beaver Bay complex, although he studied the dikes in passing rather than in-depth.

The Silver Bay site is shown in Figures 8. The granodiorite weathering stages include core stones, cobbly grus, to a coarse-grained sand size fraction of mainly disaggregated parent rock. The sample site is cross cut by calcite veins and hematite-stained fractures.

Twelve samples were collected at this site and the sampling locations are shown in Figure 8 and listed in Table 4. Sample G-12 is considered the least altered and is a sample of parent granodiorite. Samples G-3 and G-4 are grus. Sample G-7 is vein material. G-2 represents a sample that has undergone extensive alteration.

Spruce Road

Figure 9. Weathered outcrop from which a drill core, weathering rind, and grus were sampled at Spruce Road.

The site is exposed along Spruce Road in St. Louis County, MN and is part of the Vermilion district. The 2.5-2.7 Ga old Vermilion district consists of subaqueous volcanic rocks, sedimentary rocks, and intrusive granites and contain lenses of iron formation (Sims, 1976; Morey 1980). The sampling location contains multiple outcrops across the site and is part of the Duluth complex. Eleven samples were collected and include a drill core, core stones, weathering rinds, and grus.

McFarland Lake

Figure 10. Core stone with weathering rind at McFarland Lake.

The site is exposed at the side of County Road 74 in Cook County, MN which borders McFarland Lake and is approximately 2.5 miles due South of the Canadian border. The McFarland Lake saprolite is an exposure of the Logan Sills diabase. Grout and Schwartz (1933) described them as fine to medium grained with ophitic clinopyroxene and plagioclase phenocrysts.

The sampling location contains multiple sparse exposures of highly weathered outcrops and intermittently exposed veins running the length of the site. The outcrops feature core stones with pervasive onion skin weathering rinds. Veins were red-colored and easily broken by hand. The entire site was covered by a crumbly pebble to sand sized layer. Four samples were collected and include grus, onion skin weathering rind, core stone, and vein material.

Bald Eagle

Figure 11. Bald Eagle outcrop.

The site is a road cut along Highway 1 in St. Louis County, MN. The Bald Eagle Intrusion is part of the layered series of intrusions and characterized by Miller and Ripley (1996) as equal thicknesses of troctolite and gabbro. The funnel-shaped intrusion consists of high density rocks compared to surrounding anorthositic rock. The emplacement of the intrusion was between the aforementioned anorthositic series and earlier-layered South Kawishiwi and Greenwood Lake intrusions. Wahl et al. (2007) described the primary mineralogy of the Bald Eagle intrusions as consisting of plagioclase, olivine, and augite cumulates. Twelve samples were collected and include cores stones, grus, weathering rinds, and vein fill material.

Cascade River


Figure 12. Core stone, weathering rind, and interstitial material sampled at Cascade River.

The site is along a road cut in Cook County, MN off of Highway 61 near Cascade River State Park. The samples are part of the North Shore Volcanic Group described by Green (1996) as slightly siliceous basaltic andesite. The basalt flows are noted to be unusually thick. Three samples were collected: a core stone, onion skin weathering rind, and surrounding interstitial material.

Cores from DNR Core Library, Hibbing, MN

Figure 13. Drill core from the Thistledew Lake Sequence.

Cores from the DNR drill core library in Hibbing, Minnesota include samples from the Duluth Complex, the Thistledew Lake Sequence, and the Wilson Lake Sequence. The Thistledew Lake Sequence contains two units with the first consisting of mafic volcanic rocks and the second consisting of greywacke, slate, and tuff (Southwick et al., 1991). The Wilson Lake Sequence contains three units. The first unit consists of greywacke, slate, tuff, conglomerate. The second unit consists of felsic and intermediate volcanic rocks. The third unit consists of mafic to intermediate volcanic rocks (Southwick et al., 1991).

Sixty-three collected samples were prepped at UMD by washing and drying and subsampling as necessary. Samples were sent to ALS Global, Inc. where they crushed to 70% less than 2mm and riffle split 250 grams which were then pulverized to better than 85% passing 75 microns. Major oxides (whole-rock analyses, ALS analytical package ME-ICP06) were determined by inductively coupled plasma – atomic emission spectroscopy (ICP-AES). Major and trace elements (ALS analytical package ME-MS61L) were determined by fusion and aqua regia digestion and analyzed by Inductively-coupled plasma mass spectrometry (ICPMS). Analytical data are tabulated in Table xx and Appendix 1.

Table 5. List of major oxides and elements analyzed.

Oxides	Elements			
Al2O3	Ag	Fe	Ni	Th
BaO	Al	Ga	P	Ti
CaO	As	Ge	Pb	Tl
Cr2O3	Ba	Hf	Rb	U
Fe2O3	Be	In	Re	V
K2O	Bi	K	S	W
MgO	Ca	La	Sb	Y
MnO	Cd	Li	Sc	Zn
Na2O	Ce	Mg	Se	Zr
P2O5	Co	Mn	Sn	
SiO2	Cr	Mo	Sr	
SrO	Cs	Na	Ta	
TiO2	Cu	Nb	Te	

Characterization of weathering

The degree of weathering of samples was estimated using the Chemical Index of Alteration (CIA) (Nesbitt and Young, 1982) and the Chemical Index of Weathering (CIW) (Harnois, 1988). Nesbitt and Young (1982) state that the feldspars are the most abundant of the reactive minerals in the crust. During weathering, calcium, sodium and potassium are generally removed by solution. They defined the CIA as

$$CIA = [AI_2 0_3 / (Al_2 0_3 + CaO^* + Na_2 0 + K_2 0)] \times 100 \quad (1)$$

where CaO* is the amount of CaO in the silicate fraction of the rock. Harnois and Moore (1988) highlighted the fact that potassium is generally leached during soil formation. However, most Precambrian paleosols are enriched in K, indicating that potassium may be a diagenetic feature (Retallack, 1986).

Potassium is used in the formation of K-minerals, it can be adsorbed on other clays through ion exchange (owing to the higher exchange capacity of K +, the clay particles have a stronger tendency to adsorb and retain K + rather than Na + and Ca 2 +; Kronberg et al., 1986) or removed by fluid migration. Therefore, Harnois (1988) suggested that K_2O be excluded from any analysis on weathering, and proposed a CIW, where

CIW = [AI203 / (Al203 + CaO + Na20)] X 100. (2)

The CIA and CIW was calculated for all samples.

Isocon Analysis

To examine gains and losses of chemical constituents during weathering, the Isocon Analysis of Grant (1986) was employed. An isocon diagram plots an altered sample against a sample representing an original composition or least alteration, and it provides a graphical means of expressing changes in mass volume or element mobility (Grant, 1986). The isocon is defined by immobile species that plot on a straight line though the origin, typically SiO_2, Al_2O_3, and TiO_2 are considered immobile, although other species may be appropriate.

Isocons were defined from geochemistry results plotting most and least altered samples at each site to illustrate mobility of cations and oxides during the weathering process (Grant, 1986).

X-Ray Diffraction and Characterization of Weathering

Returned pulps from ALS Global, Inc. processing, provided the material for XRD analyses. A split of each sample was added to a column of distilled water with sodium heximetaphosphate added as a dispersant. Mixtures were allowed to settle and a coarse-fraction (<62 μm) and a fine fraction (<2 μm) were withdrawn to make a wet-mounted slide. Stokes's Law was used to determine settling velocities for sediment in a liquid column:

$$v = \frac{2}{9}\frac{(\rho_p - \rho_f)}{\mu} g R^2, \quad (3)$$

where v is the velocity, ρ_p is the mass density of the particle, ρ_f is the mass density of the fluid, μ is the dynamic viscosity, g is gravity, and R is the radius of the particle. Fine fractions were removed after 15 minutes from a depth of 1 cm according to Stokes's Law and made into wet-mounted slides to amplify the clay fraction for identification analysis. Sodium hexametaphosphate as a dispersant was added to select

samples to properly disperse clay fractions for XRD scan analysis. Powder mounts were made from the remaining pulps.

To determine clay mineralogy slides and powder mounts were run on a Rigaku MiniFlex300 X-ray diffractometer using CoK_{α} at wavelength v = 1.709010Å and a PANalytical X-ray Diffractometer using CuK_{α} at wavelength v = 1.541874Å as quick-scans in the 2θ range from 5° to 65° at 0.066667°/s and a step size of 0.01 and reviewed using Match! analytical software to quickly identify samples with clay size particles for longer, more detailed scans from 2.15° to 35° at 0.01 °/s and a step size of 0.005 on the PANalytical X-ray Diffractometer. Coarse, fine, and powder scans were compared to determine relative abundances of clay minerals. Samples that were selected for longer scans were subjected to vapor glycolation at 60°C for 8 hours for smear slides and 12 hours for powder mounts and scanned immediately upon removal from the oven to identify specific clay mineralogies. These samples were also heated to 550°C for one hour to observe peak shifts and identify clays. Table 6 below lists basal reflections of a pure sample of various clays.

Table 6. Clay mineral low angle reflections with ethylene glycol and heat treatments.

Clay	Air-Dried (2θ)	Ethylene Glycol	Heated to 550°C
Kaolinite	12.6	No change	Peak Collapse
Smectite (Na)	6.55	4.78	8.85
Smectite (Ca)	5.43	4.78	8.85
Chlorite	6.3	No change	No change
Illite	8.85	8.85	8.85

RESULTS

Calculated CIA and CIW values were plotted (Figure 14) to compare weathering indices across outcrops. The sites fell along a similar trendline with the exception of the Silver Bay outcrop, which was a granophyre. Crow Creek and Silver Bay were chosen for more in-depth study based on completeness of weathering profile among samples.

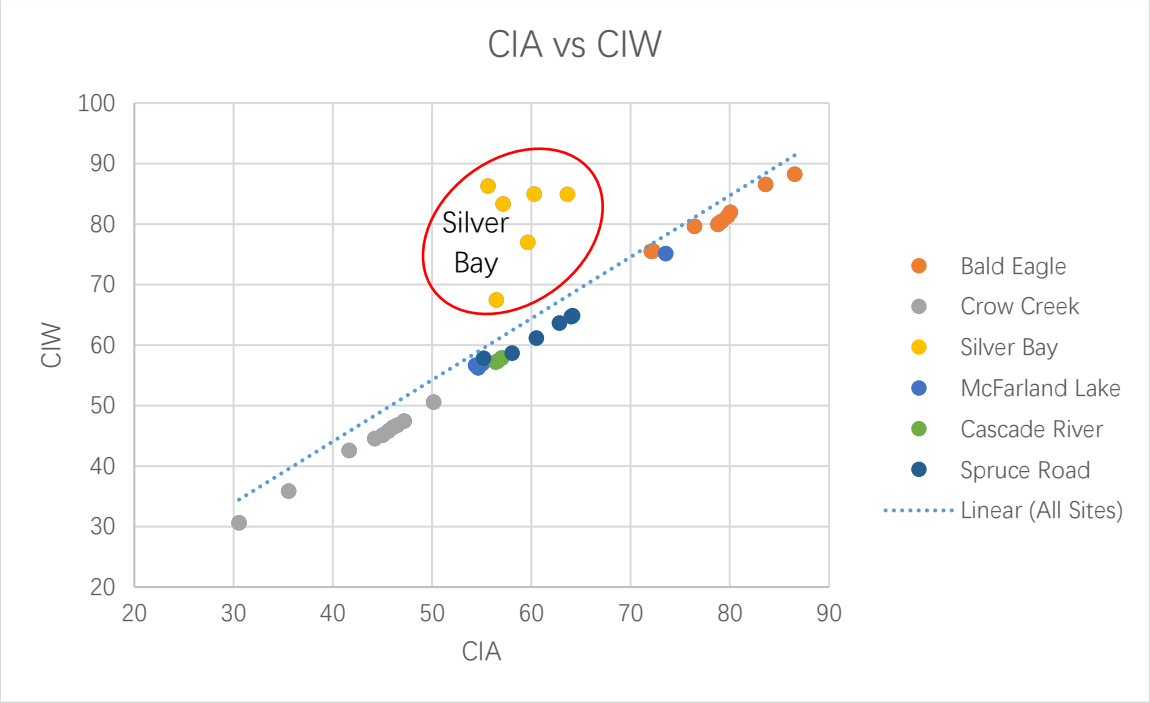

Figure 14. Outcrop site CIA and CIW comparisons. The chart illustrates that the more mafic sites follow a similar weathering indices trendline, while the Silver Bay granophyre is clustered above the trendline.

Crow Creek Site

At Crow Creek, the unaltered diabase is composed of plagioclase, orthopyroxene, clinopyroxene, feldspar, olivine, magnetite, and accessory minerals. The altered rock mineralogy is quartz, chlorite, talc, laumontite, prehnite, smectite, kaolinite, and illite.

After geochemical analysis, samples collected from Crow Creek were evaluated for their degree of alteration or weathering using visual inspection and loss on ignition data. Four samples were selected as best illustrating element and oxide mobility during alteration and are shown in Table 7 below. A scaling factor was applied for oxides for visual clarity on the isocons, particularly for oxides with exceptionally high or low values so that they would be legibly displayed.

Table 7. Oxides of selected Crow Creek samples.

	CC-3	CC-11	CC-9	CC-8	Scale
Oxide	Core Stone	Core Stone	Vein Adjacent Material	Vein Fill	(Applied after)
SiO2	48.2	46	46	48.6	0.33
Al2O3	21.8	20.2	18.95	17.25	1
Fe2O3	8.31	9.62	8.83	1.94	5
CaO	11.55	10.65	9.68	12.45	3
MgO	4.95	6.14	7.09	2.81	5
Na2O	2.56	2.2	2.06	0.39	15
K2O	0.28	0.22	0.19	0.83	20
Cr2O3	0.015	0.018	0.016	0.004	1000
TiO2	0.93	0.95	0.92	0.13	20
MnO	0.12	0.12	0.13	0.04	100
P2O5	0.09	0.09	0.08	0.02	100
SrO	0.04	0.03	0.03	0.02	100
BaO	0.01	0.01	0.01	0.01	500
Total	101.99	99.84	100.69	99.53	-
LOI	3.1	3.6	6.7	15.1	2
CIA	46.1	46.5	47.2	41.6	
CIW	46.4	46.8	47.5	42.6	

CC-3 is a core stone within the original diabase sill and was chosen as the least weathered end member; this sample had the lowest LOI and CIW. CC-11 is also a core stone but determined to be slightly

more altered than CC-3, because of its slightly higher LOI, and CIW. CC-9 is a highly grussified material adjacent to a highly altered vein, sample CC-8, which is the fill from a highly altered vein adjacent to CC-9. Isocon diagrams were made plotting the least weathered sample against successively more weathered samples and applying a scale (Table 7) to show depletion and enrichment of oxides and elements. Isocon plots were made, using the major oxides (Figure 15A, 14B, 14C).

Oxides appearing below the isocon are depleted by weathering and oxides above the isocon are enriched. When compared to an unaltered or parent sample, a least altered sample will have oxides on or near the isocon. The more altered a sample is, the more dispersed both above and below from the isocon its oxides will be.

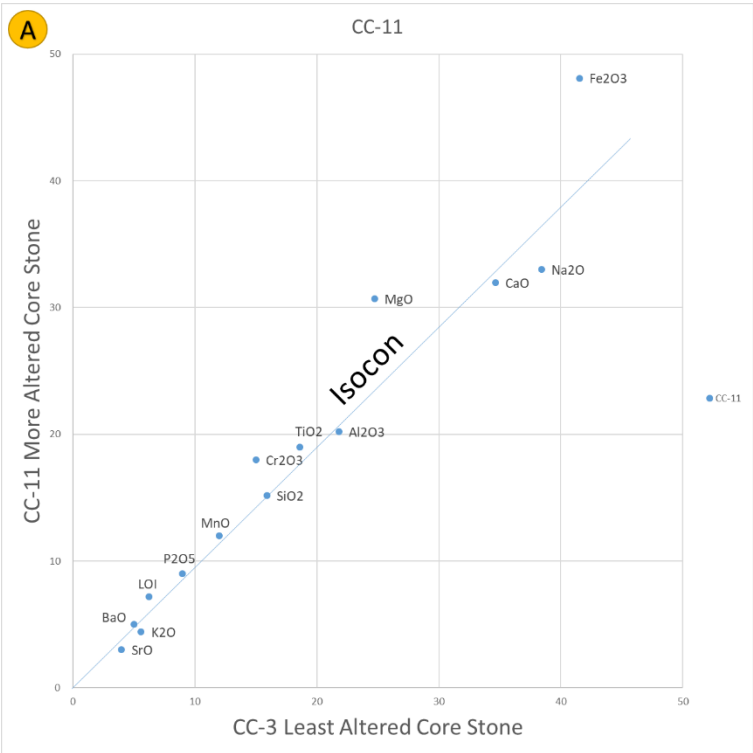

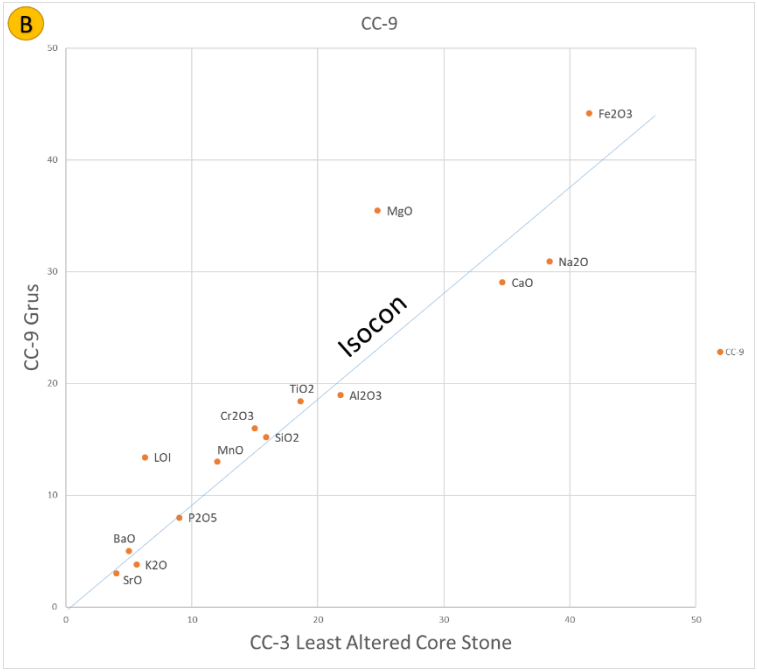

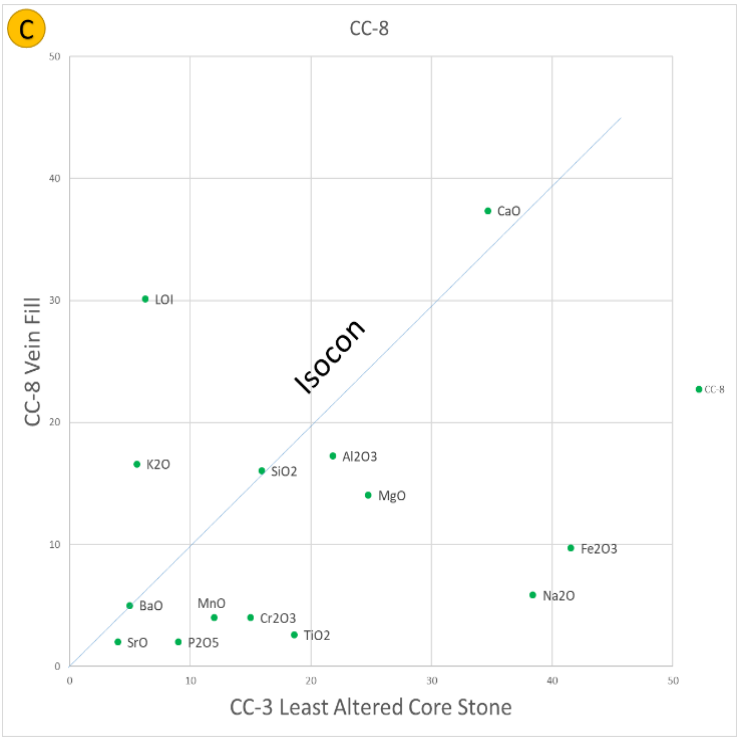

Figure 15. Isocons of the major oxides at Crow Creek.

The isocons plot a least altered core stone end member, CC-3, against (A) CC-11, a more altered core stone; (B) CC-9, grus; (C) CC-8, vein fill. Scaling factors used for plotting are listed in Table

7. Oxides plotting above the isocon are enriched or concentrated; oxides plotting below the isocon are depleted.

Figure 15 (A) is an isocon plot of the least altered core stone (Figure 5) compared to a more altered core stone (Figure 6). Using SiO_2 and Al_2O_3 as immobile elements to define the isocon, the slightly more altered sample shows a slight loss of K_2O and Na_2O and small gains of Fe_2O_3 and MgO. Loss on ignition is similar between the two samples.

Figure 15B, least altered (CC-3, Figure 5) vs. Grus (CC-9, Figure 6), shows continued loss of K_2O, Na_2O, and CaO, with greater MgO and Fe_2O_3 gain at this stage of grus development. Figure 15C, least altered (CC-3, Figure 5) vs. vein material (CC-8, Figure 6), indicates a significant change in alteration assemblage. Al_2O_3 and TiO_2 are both depleted. Therefore SiO_2, which lies on the 1:1 ratio, was used to define the isocon. Na_2O, Fe_2O_3, MgO, and TiO_2 are highly depleted, whereas K_2O is significantly enriched. Loss on ignition is also significantly greater than the unaltered sample suggesting a hydrated mineral phase.

X-Ray Diffraction

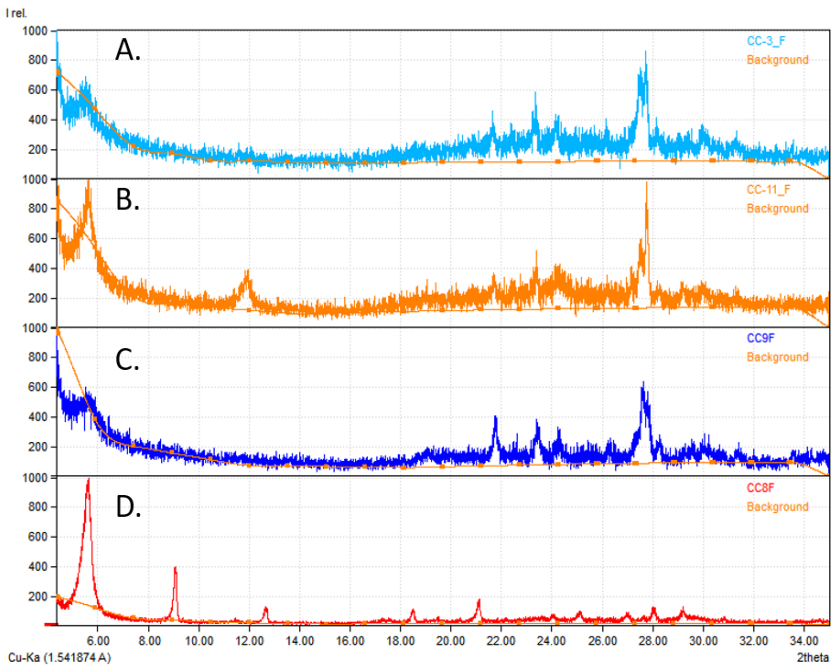

Figure 16. Diffractogram of the selected fine sediment samples from Crow Creek.

Scans are from least to most altered from the top down: A. core stone (CC-3, Figure 5), B. altered core stone (CC-11, Figure 6), C. vein adjacent grus (CC-9, FIgure 6), and D. vein fill (CC-8, FIgure 6) from Crow Creek from 5-35° 2θ.

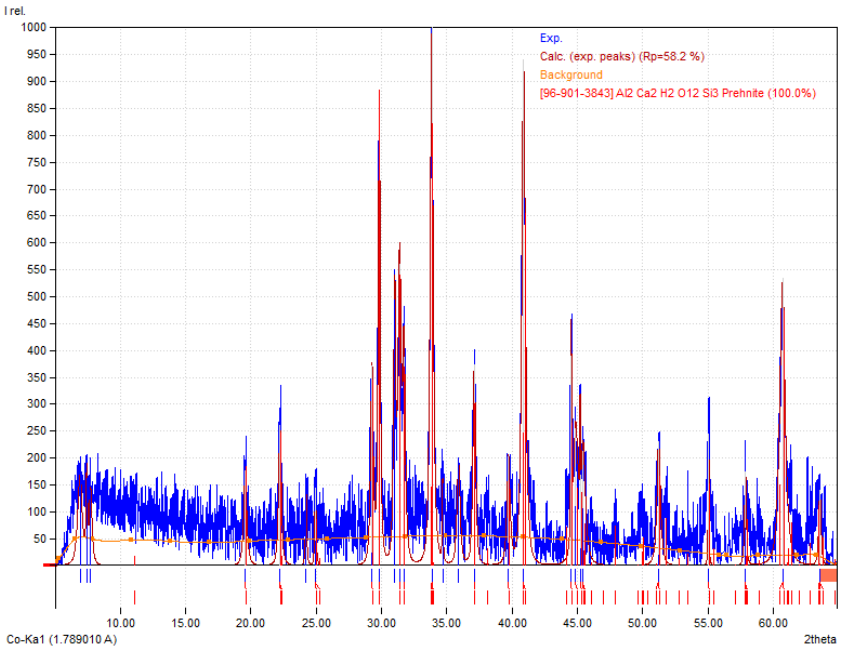

Figure 17. Diffractogram of prehnite grain from Crow Creek.

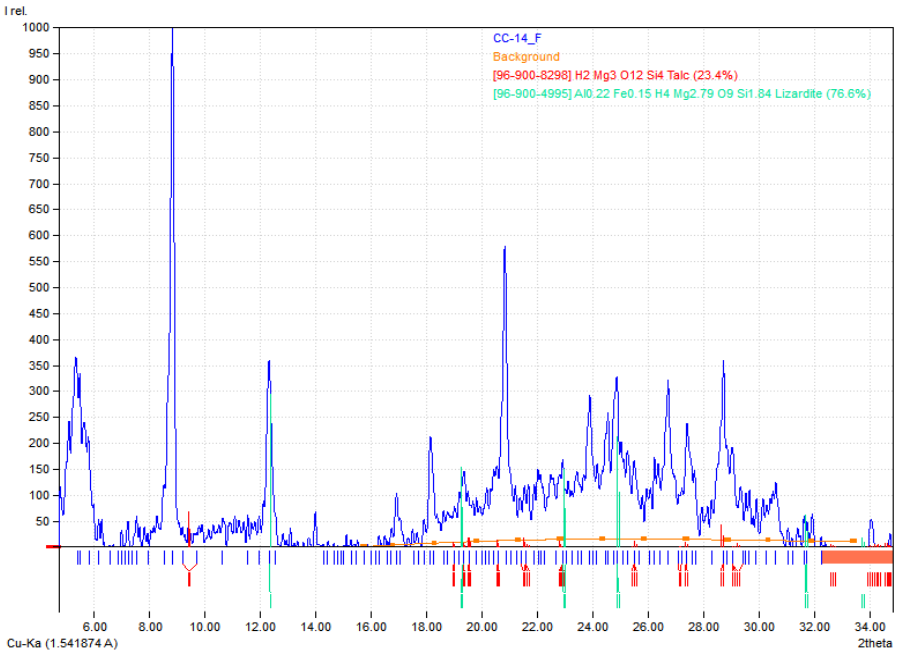

Figure 18. Diffractogram of lizardite (serpentine) and talc.

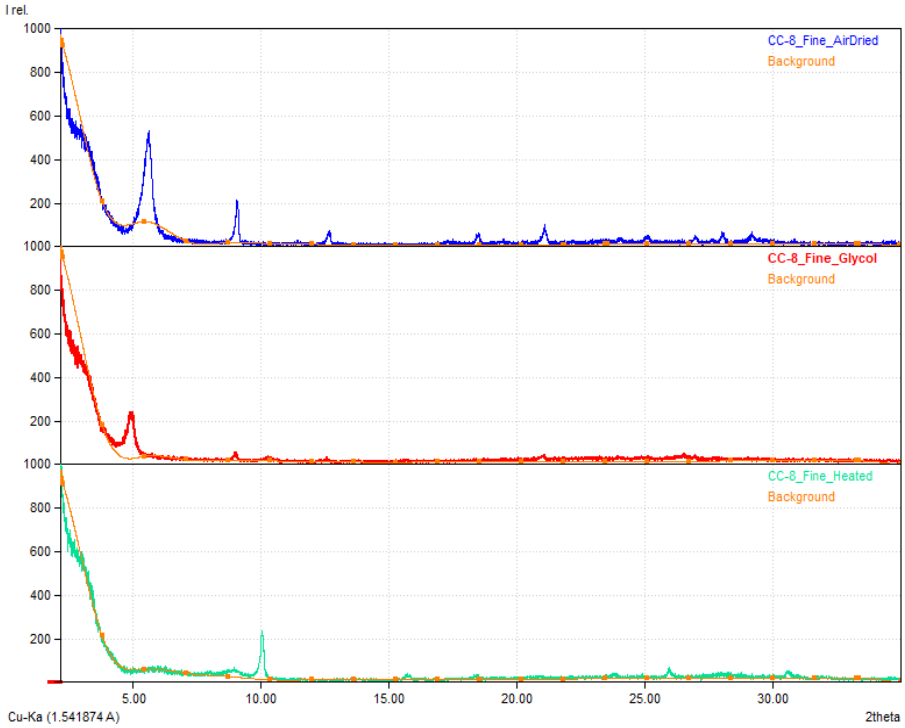

Figure 19. Air-dried, glycolated, and heated diffractogram patterns of Crow Creek vein fill.

X-ray diffractogram patterns showed primary feldspars, pyroxenes, olivine, biotite, amphibole (Figure 15, A,B,C,D). Several secondary minerals were identified, including quartz, talc (CC-14), laumontite (CC-3, Figure 5), prehnite, serpentine (lizardite) (CC-14), and iron oxide. Clay minerals were identified in sample CC-8 (Figure 19). Samples contained relatively little clay with peaks often just over 100 counts per second above background. However, some clays were identified in vein fill material. Clays identified were smectite, kaolinite, chlorite, and illite. Smectite was found in highly grussified samples and vein fill. Ethylene glycol treatment causes the 5.7 to 6.3 2-theta spacing of smectite to expand to 8.85 2-theta as the ethylene glycol penetrates the clay interlayer spaces, illustrated in Figure 19. Kaolinite is a non-expansive clay which fails to respond to glycolation and whose 12.6 2 theta spacing collapses upon heating to 550 ˚C as shown in Figure 19. Illite and chlorite do not respond to glycolation. Illite does not respond to heating. The chlorite peaks occupy similar spacing to kaolinite (7 Å, ~12.6 2θ) or smectite (14 Å to 15 Å, ~5.7 to 6.3 2θ) but may sharpen upon heating instead. Kaolinite, chlorite, illite were only observed in vein fill material (Figure 19).

CIA and CIW indices indicated the vein adjacent material was the most highly weathered, while vein fill was the least. CIA and CIW indices indicate the degree of weathering of silicate materials, however CIA and CIW may not always accurately reflect the degree of weathering in hydrothermal alteration or metamorphism environments due to changes in bulk chemistry. Visual inspection, LOI, Isocon and XRD analyses all show the vein material as being the most highly altered sample.

Silver Bay

Hand samples from the Silver Bay granophyre site were collected for analysis that included unaltered granophyre (G-12), altered rock (G-1, G-2), grus (G-3, G-4), and vein fill material (G-7). Four additional samples were collected in a second site visit to verify X-ray Diffraction results that were not subjected to geochemical analysis including a highly grussified sand (G-13). Veins of calcite were common throughout the outcrop as is iron staining. Near the top of the exposure iron oxide staining is common along the margins of fractures. Hand sample examination of the outcrop defined the parent rock as a granophyre, with identified minerals of K-feldspar, augite, apatite, plagioclase, quartz and calcite.

Samples were evaluated for their degree of alteration or weathering using visual inspection and loss on ignition data. Four samples were selected as best illustrating element and oxide mobility during alteration and are shown in Table 8 below. A scaling factor was applied to oxides for graph legibility on the isocons, particularly with oxides that had exceptionally large or small values.

Table 8. Oxides of selected Silver Bay samples.

	G-12	G-4	G-7	G-2	Scale
Oxide	Unaltered	Grus	Vein Fill	Rock/Calcite	(Applied after)
SiO2	64.9	62.9	58.7	22.8	0.33
Al2O3	11.95	11.75	9.95	3.62	0.5

Fe2O3	10.25	9.11	8	1.23	1
CaO	0.82	1.96	7.51	38.5	0.6
MgO	2.22	1.35	0.85	0.51	10
Na2O	3.51	1.27	1.21	0.39	5
K2O	3.17	4.27	5.05	1.61	2
Cr2O3	0.003	0.004	0.005	0.003	750
TiO2	0.81	0.79	0.56	0.22	10
MnO	0.21	0.1	0.26	0.07	20
P2O5	0.09	0.1	0.07	0.03	40
SrO	0.01	0.01	0.01	0.01	1
BaO	0.1	0.1	0.1	0.03	20
Total	100.38	99.1	100.52	100.12	-
LOI	2.34	7	8.24	31.1	3
CIA	56.5	59.7	57.2	60.3	
CIW	67.4	77.0	83.3	85.0	

G-12 is an unaltered sample from the parent rock, and is used as the least weathered end member (Figure 8). G-4 is grusified granophyre located along the margin of the weathering pendant immediately adjacent to core stones (Figure 8). G-7 is material fill from a vein from the middle of the weathering pendant. G-2 is a rock with several calcite veins to the right of G-4 grus. Additional samples were collected on a second visit to verify XRD results and were not subjected to geochemistry, among them is

sample G-13 which was highly grussified material to the left of G-4 in Figure 8. Isocons were made plotting a scaled least weathered sample against successively more weathered samples to show depletion and enrichment of oxides and elements.

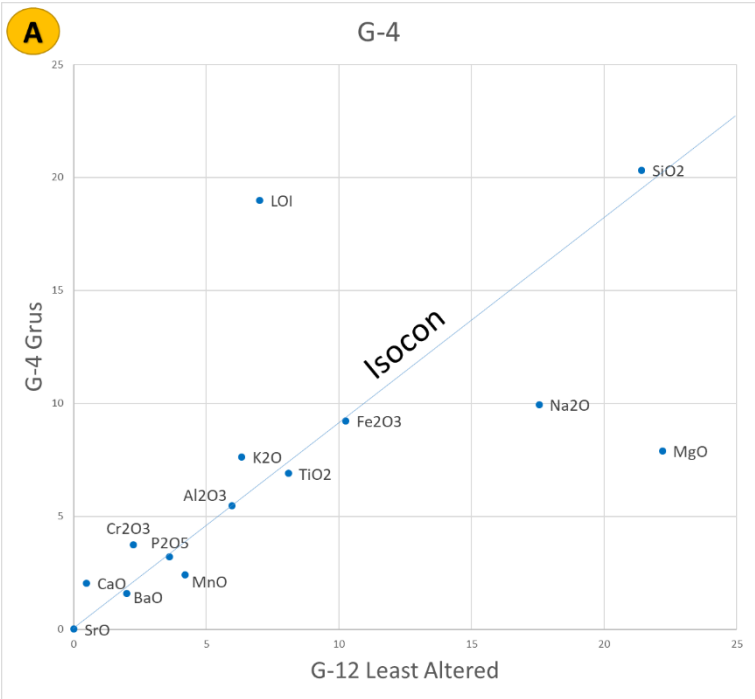

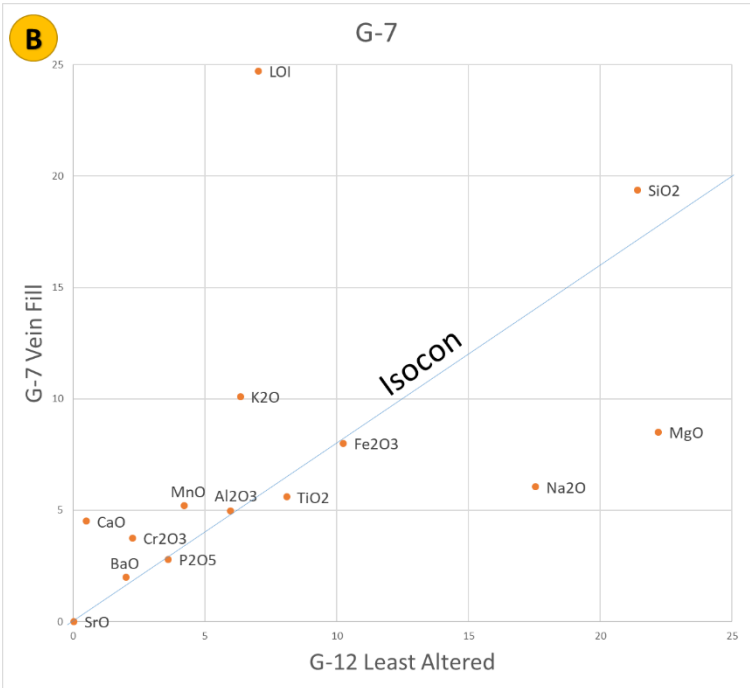

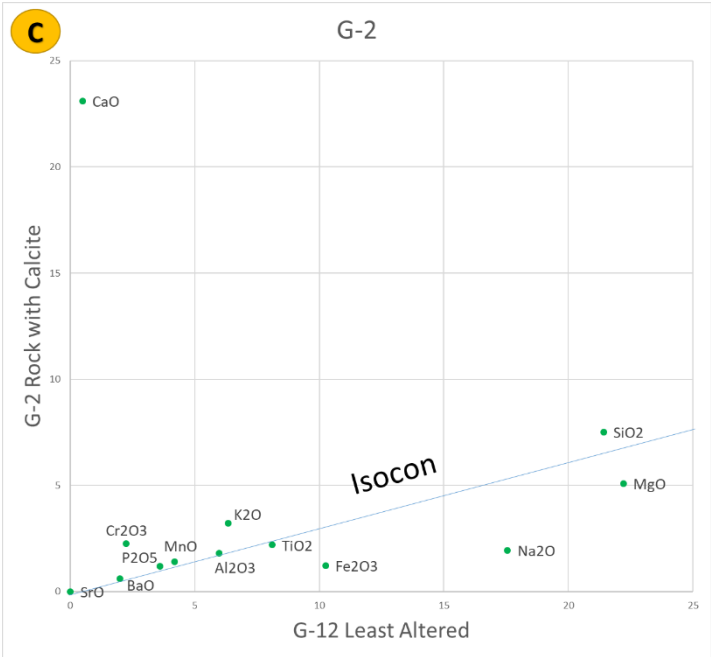

Figure 20. Isocons of the oxides from Silver Bay.

Isocons plot a least altered core stone end member (G-12) plotted against (A) G-4, cobble-sized grus; (B) G-7, vein fill; (C) G-2, highly altered rock. Scaling factors used for plotting are listed in Table 8. Oxides plotting above the isocon are enriched or concentrated; oxides plotting below the isocon are depleted.

Figure 20A, B, and C shows depletion progression of weathering from the unaltered granophyre (G-12), to the grus, then to the vein fill material. The isocon is defined by Al_2O_3 and Fe_2O_3 and the analysis indicated progressive loss of MgO and Na_2O, gains in K_2O and CaO, and increasing LOI (Figures 19A and 19B). The vein also shows some enrichment of MnO (Figure 20B). Figure 20C shows significantly greater enrichment of CaO in the altered rock, which in this case is approximately 50% calcite; the progression of weathering is accompanied by calcite deposition. Figure 20 also shows additional depletion of Fe_2O_3 in the altered sample relative to the unaltered granophyre.

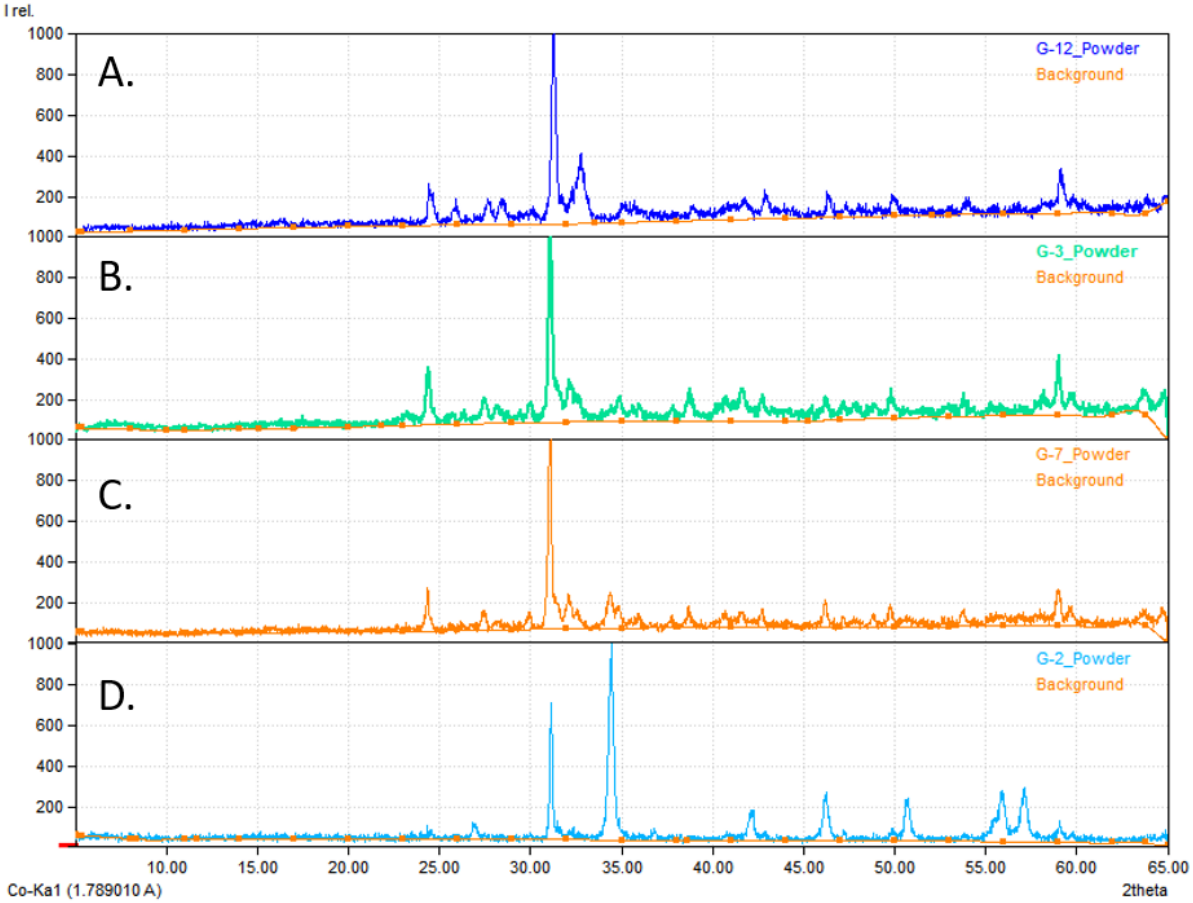

Figure 21. X-Ray Diffraction of granophyre powder samples.

Figure 21 is a diffractogram of the selected powder samples from the granophyre. Scans are from least to most altered from the top down: unaltered drill core (G-12), grus (G-3), vein fill (G-7), highly altered rock (G-2) (Figure 21). Samples G-12, G-3, and G-7 are similar in bulk composition; however, G-2 highlights the high calcite content.

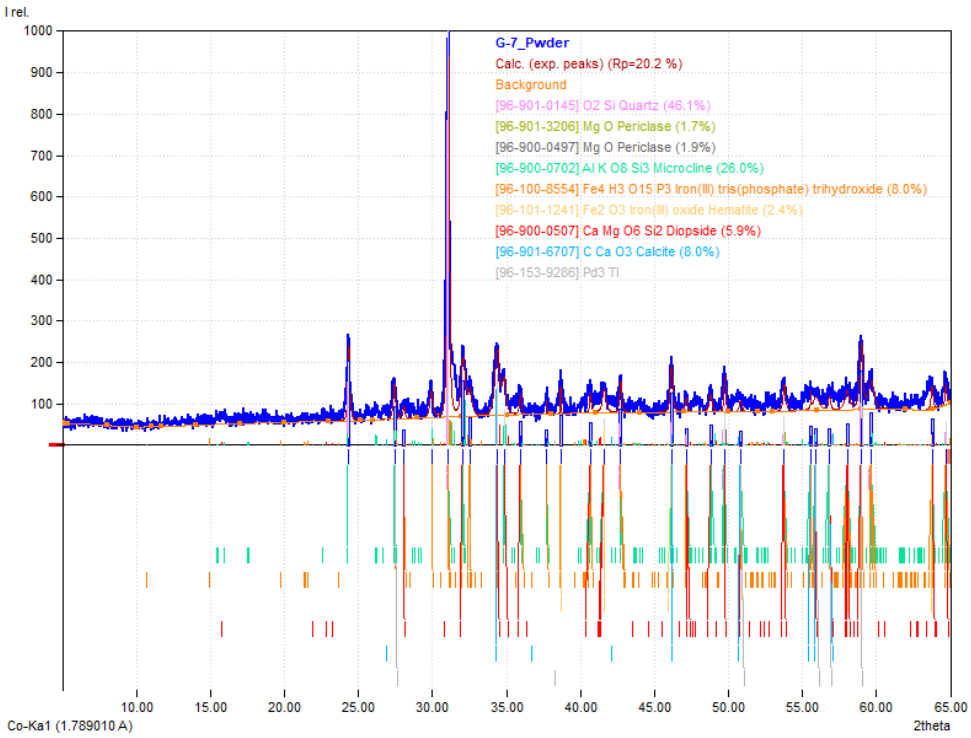

Figure 22. XRD patterns of feldspars, augite, apatite, calcite, quartz, Fe-oxides, Fe-Ti oxides, and kaolinite.

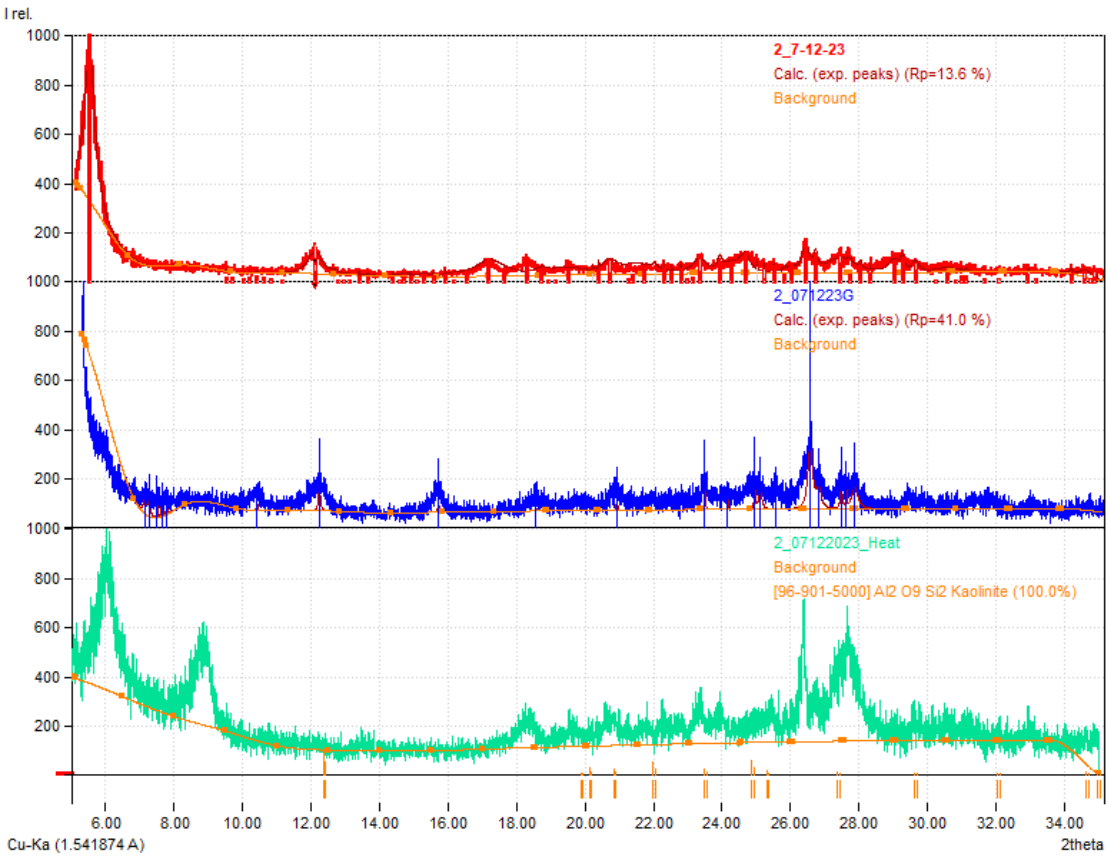

Figure 23. Air-dried, glycolated, and heated diffractogram patterns of Silver Bay granophyre.

Figure 23 shows highly grussified material, G-13, smectite peak response to glycolation and heat; Kaolinite peak that collapses upon heating.

DISCUSSION

Typical weathering of igneous rocks follows Goldich's (1938) dissolution series, with mafic minerals having a lower stability threshold at surface conditions than intermediate, followed by the most stable, felsic. Mafic weathering progressions typically start with a parent material composed of plagioclase, pyroxene, and olivine, which will weather to smectite group and kaolinite group clay end products (Nesbitt and Wilson, 1992). As rocks move from mafic to felsic, the weathering products gradually include more chlorite, aluminum oxides, and quartz grains (Wilson, 2004).

Iron-bearing minerals at the Crow Creek site, which include olivine and pyroxene, are more readily weathered being particularly susceptible to acidic conditions and oxidation (Goldich, 1938; Wilson, 2004). The weathering progression at Crow Creek indicates progressive loss of Na_2O and CaO, gain of K_2O, and increasing proportions of hydrated mineral phases indicated by increasing LOI (Figure 15A, 14B, 14C). Clay minerals including illite and kaolinite are found in the most altered samples (CC-8, Figure 19).

The isocon geochemistry in Figure 15A showed minor enrichment of Fe_2O_3, MgO, and Cr_2O_3 in the altered core stone and grus and some leaching of Na_2O associated primarily with pyroxene weathering and accessory mafic minerals. The enrichment of MgO and Cr_2O_3 in the altered sample could be attributed to the percolation of fluid from a more weathered horizon above transporting mafic oxide-elements to the altered core stone. Fe_2O_3 is generally considered immobile during weathering and generally increases due to the depletion of other elements (Colman, 1982). Figure 15B has a less tightly defined isocon, but indicates a similar process was in effect for the grus. MnO is more soluble under higher pH conditions than Fe (Herndon et al., 2011), but may be enriched via hydrothermal activity in rift zones (Roy, 1997). CaO leaching was observed in the grus that is likely from the onset of feldspar weathering. The vein fill in Figure 15C showed enrichment of K_2O and depletion of most oxides, suggesting partial dissolution of feldspars with more potassic feldspars remaining intact.

X-ray diffraction of samples at Crow Creek identified primary mineralogy remained even in the most weathered sample. Products of olivine and pyroxene weathering found in XRD include iron oxides, serpentine (lizardite), and talc. Iron oxides form through oxidation and occur early in weathering. Olivine produces iron oxides such as hematite through a series of reactions.

Oxidation of Fayalite (Iron end-member olivine) (Earle, 2015).

$$Fe_2SiO_4 + 4H_2CO_3 \rightarrow 2Fe_2 + 4HCO_3^- + H_4SiO_4^- \qquad (4)$$

fayalite carbonic acid carbonate silicic acid

Iron to hematite (Earle, 2015).

$$2Fe^{2+} + 4HCO_3^- + \frac{1}{2}O_2 + 2H_2O \rightarrow Fe_2O_3 + 4H_2CO_3$$

bicarbonate hematite carbonic acid (5)

Serpentine is a product common to hydrothermal metamorphism and retrograde metamorphism with the lizardite and chrysotile phases being particularly associated with low temperatures of stability, below 300°C (Schwartz et al. 2013; Alderton, 2020).

Generalized olivine dissolution reaction (adapted from Lamadrid et al., 2017).

$$2(Mg, Fe)_2SiO_4 + 4H^+ \rightarrow Mg^{2+} + Fe^{2+} + SiO_2 + 2H_2O$$

olivine quartz(aq) (6)

Precipitation of serpentine reaction (Lamadrid et al., 2017).

$$3Mg^{2+} + SiO_2 + 2H_2O \rightarrow 5Mg_3Si_2(OH)_4 + 6H^+$$

quartz(aq) serpentine (7)

Talc forms from early alteration of olivine at depth through magmatic and metamorphic processes and can often be found in relatively fresh rock (Wilson, 2004). Talc was likely formed by metamorphism during emplacement. XRD scans additionally identified chlorite and smectite which are common secondary products along with Mg^{2+}, Ca^{2+}, and Fe^{2+} dissolved ions from pyroxene partial dissolution (Huang and Wang, 2005).

Generalized serpentine to talc reaction (Moore and Rymer, 2007).

$$2Mg_3Si_2O_5(OH)_4 + 2SiO_2 \rightarrow Mg_2Si_4O_{10}(OH)_2 + 3H_2O$$

serpentine quartz talc (8)

Pyroxene may also react under hydrous conditions to form serpentine and talc.

Pyroxene (enstatite) to serpentine and talc reaction (Frost and Beard, 2007).

$$6MgSiO_3 + 3H_2O \rightarrow Mg_3Si_2(OH)_4 + Mg_3Si_4O_{10}(OH)_2$$

enstatite serpentine talc (9)

XRD scans also identified chlorite, prehnite, and laumontite, a zeolite. Chlorite and prehnite are formed via replacement of plagioclase and the secondary mineral serpentine.

Simultaneous replacement by chlorite and prehnite (Nozaka et al., 2017).

$$5Mg_2SiO_4 + 4CaAl_2Si_2O_8 + 10H_2O \rightarrow 2Mg_5Al_2Si_3O_{10}(OH)_8 + 2Ca_2Al_2Si_3O_{10}(OH)_2$$

serpentine plagioclase chlorite prehnite (10)

$$6CaAl_2Si_2O_8 + 5Mg_3Si_2O_5 + 5H_2O \rightarrow 3Ca_2Al_2Si_3O_{10}(OH)_2 + 3Mg_5Al_2Si_3O_{10}(OH)_8 + 4SiO_2$$

plagioclase serpentine prehnite chlorite quartz(aq) (11)

The formation of laumontite marks the lowest-grade metamorphism (Zhao, 2021). The presence of both a laumontite and prehnite indicate incipient or burial metamorphism of mafic rocks across the zeolite facies to the prehnite-pumpellyite facies (Frost, 1980). Tschernich (1992) described the rate of formation of laumontite as being highly temperature-dependent, often forming layered temperature zones of minerals. Laumontite formation is commonly seen at depths between 3-5 km and restricted primarily by temperatures of 110-190°C (Cho et al., 1986; IIjima, 1995).

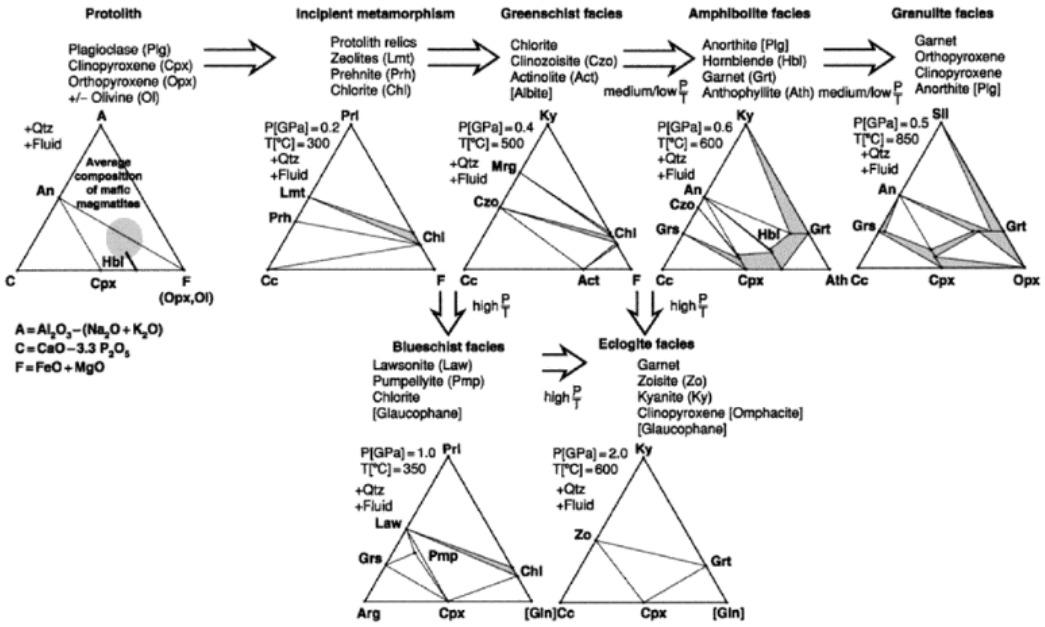

Figure 24. Hoinkes et al. (2005) illustrated incipient metamorphism diagram.

In Figure 24, Hoinkes et al. (2005) illustrated incipient metamorphism mineralogy consistent with mineralogy observed at Crow Creek in the second triangle on the top row .

The particular assemblage of laumontite-prehnite-chlorite constrains the formation environment to pressures below 0.3 GPa and temperatures of 300°C consistent with volcanic and plutonic regions (Hoinkes et al., 2005).

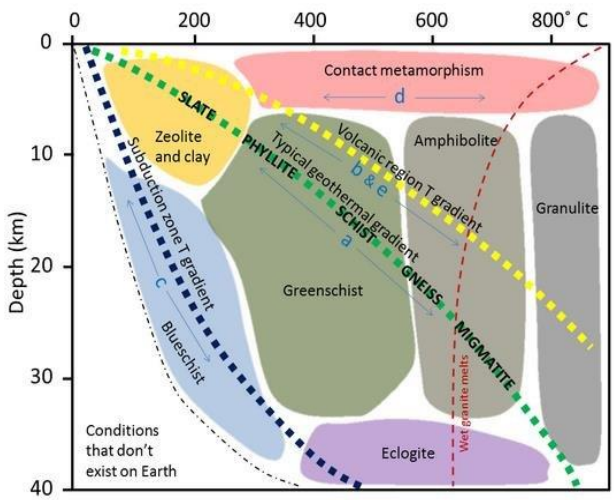

Figure 25. Temperature-Pressure diagrams illustrating thermal gradients of zeolites from Kuethe, 2016.

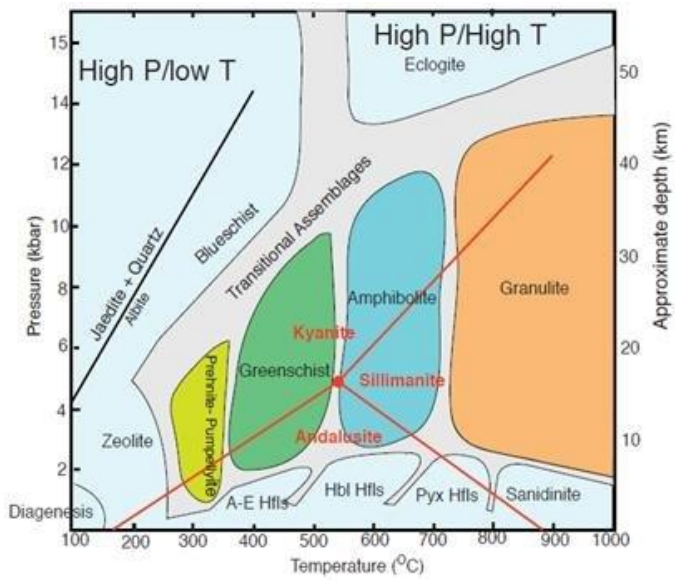

Figure 26. Temperature-Pressure diagrams illustrating thermal gradients of prehnite from Kuethe, 2016

Figures 25 and 26 from Kuethe (2016) show ranges for Zeolite to prehnite transitions which occur at low pressures and temperatures.

This laumontite-prehnite-chlorite combination in the diabase sill suggests that it was originally emplaced at a depth of approximately 3-5 km and underwent retrograde metamorphism. Prehnite and chlorite likely formed first at higher temperatures between 210°C upwards to 400°C (Seki and Lou, 1981) followed by laumontite as the sill cooled.

XRD identified Crow Creek clays in altered samples of highly altered grus and veins. Smectite appeared in samples collected from locations adjacent to veins and vein fill, with kaolinite and illite appearing only in vein fill. Feldspar to kaolinite formation rates are often considered to be a slow process on the order of thousands to millions of years of fluid-rock interactions in natural environments (White and Brantley, 2003; Zhu, 2005; Zhu et al., 2006; Yuan et al., 2019). Dill (2016) describes kaolinite as having a wide variety of formation environments and parent lithologies but notes an upper limit of 390°C for formation. Feldspars weather when exposed to acidic waters through hydrolysis to produce primarily kaolinite clay and dissolution to produce K^+, Na^+, and Ca^{2+} ions. The weathering of feldspar into kaolinite is formulaically described below.

Dissolution of feldspar (adapted from Bohn et al., 2015).

$$(Na^{+}, Ca^{2+}, K^{+})Al_{(1-2)}Si_{(2-3)}O_8 + H_2O + H^{+} \rightarrow Na^{+} + Ca^{2+} + K^{+} + Al^{3+} + Si(OH)_4(aq)$$

feldspar soluble silica (12)

Hydrolysis of feldspar to kaolinite clay (adapted from Appelo and Postma, 2004).

$$2KAlSi_3O_8 + 2H^{+} + H_2O \rightarrow Al_2Si_2O_5(OH)_4 + 2K^{+} + 4SiO_2(aq)$$

K-feldspar kaolinite quartz(aq) (13)

The potassium feldspar represents the only major source of potassium from the unaltered rock at this site.

The smectite that was identified in scans can form through weathering pathways from a variety of igneous minerals to include but not limited to olivine, pyroxene, and feldspars (Baker and Haggerty, 1967; Velbel and Barker, 2008; Altaner, 2013; Kloprogge et al., 1999). Multiple species of smectite can also be sources of kaolinite in hydrothermal fluids with higher H^{+} conditions (Karathanasis and Hajek, 1983; Fulignati, 2020).

Illite was also observed in XRD scans. Illite forms from silicate weathering, such as feldspar, through the illitization of smectites or via the reaction of K-feldspar and kaolinite (Huggett, 2005). Illitization of kaolinite takes place at depths of 3-4 km (Mantovani et al., 2010) and illitization of smectite occurs at depths of 2.5-3.5 km (Qin et al., 2019) with increasing illite and decreasing kaolinite and smectite with greater depths.

Illitization of kaolinite reaction (Xiao et al., 2018).

$$KAlSi_3O_8 + Al_2Si_2O_5(OH)_4 \rightarrow + KAl_3Si_3O_{10}(OH)_2 + SiO_2(aq) + H_2O$$

K-feldspar kaolinite illite quartz(aq) (14)

Illitization of smectite reaction (adapted from Hugget, 2005).

$$(Na, Ca)_{0.33}(Al, Mg)_2Si_4O_{10}(OH)_2 \bullet (H_2O)\text{n} + K^+ + KAl_3Si_3O_{10}(OH)_2 + ions$$

smectite illite (15)

The results of the geochemical analysis and XRD scans of prehnite-laumontite-chlorite and illite are consistent with weathering of a diabase intrusion at 3-5 km
depth.

Silver Bay Site - Granophyre Weathering

The iron-bearing minerals within the granophyre were augite with minor to rare olivine. The Silver Bay site geochemistry showed early leaching of MgO and Na_2O and slight enrichment of Cr_2O_3 and due to augite and accessory mineral weathering in Figure 20A. Augite weathering formed calcite, hematite, and quartz.

Augite to calcite, hematite, and quartz generalized formula (adapted from Rani and Shrivastava, 2016).

$$2(Na, Ca)(Al, Mg, Fe, Ti)(Si, Al)_4O_6 + H_2CO_3 \rightarrow SiO_2 + CaCO_3 + Fe_2O_3 + H_2O \ {}^{+}/_{-}\ ions$$

augite carbonic acid quartz vcalcite hematite (16)

Enrichment of K_2O and leaching of Na_2O suggests feldspar dissolution has begun (Formula 12). CaO is normally leached prior to Na_2O in feldspar weathering, however calcite deposition was observed to be ubiquitous throughout the weathering profile leading to higher CaO in all weathered samples. Figure 20B shows greater enrichment of K_2O and CaO in the vein with progressed feldspar dissolution and calcite deposition. Figure 20C shows the altered rock is greatly enriched in CaO due to

calcite deposition from hydrothermal fluids. Fe_2O_3 has been leached from the vein fill material with progressed weathering of augite.

XRD results for the granophyre returned quartz, feldspar, apatite, augite, calcite, and Fe-oxides shown in Figure 21A (G -12) and Figure 22 (G-7).

Match! XRD analysis software returned a result of kaolinite depending on parameters input to software and sample peaks had exceptionally low counts per second, suggesting very little clay development. Additional samples were collected from the site to corroborate the initial kaolinite results, which were not subjected to geochemical analysis. The most representative sample is seen in G-13 (Figure 23) which showed kaolinite and smectite peaks. Smectite can form from the weathering of variety of igneous minerals while kaolinite can develop from dissolution of feldspars (see Formula 12) or from smectite in hydrothermal fluids with high H^+.

CONCLUSION

The goal of this study was to characterize the weathering of mid-continent rift rocks in an attempt to understand the nature of the weathering, the geologic environment, and the history of the craton. The rock units studied in depth were a diabase sill from Crow Creek and a granophyre intrusion near Silver Bay. Interpretations have been made based on prior research, geochemistry and XRD results.

In Minnesota, saprolites have been recorded throughout the state at various depths in drill cores and often in multiple events within the same drill core. There are at least six known unconformities in the stratigraphy of the state of Minnesota recorded in the Animikie basin in the north and the Paleozoic to Cenozoic sediments in the south. The sediments that are preserved only account for approximately 25% of geologic time.

The weathering of the craton has a long and complicated history. Weathering horizons were observed on the Saganaga tonalite that were developed during the Archean (Davidson, 1980; Lodge et al., 2013). The Lorrain Formation records a weathering event from the early Proterozoic (Robertson and Card,

1972; Rainbird et al., 1990; Young, 2013; Bekker, 2015; Young, 2019). Superior-type iron formations, which were a product of weathering and erosion, were also deposited during the early Proterozoic (Nesbitt and Young, 1982; Purucker, 1983; Rainbird et al., 1990; Fedo et al, 1997; Ojakangas et al., 2001b; Young, 2002; Klein, 2005; Pietrzak-Renaud; 2013; Eriksson and Condie, 2014; Young, 2019). Additional weathering events were estimated to occur from 950 to 600 Ma in southern Ontario, Canada (Turek and Robinson, 1984). Farley and McKeon's (2015) dates of supergene enrichment in the Gogebic iron range in Michigan at 772 Ma and 453 Ma suggest widespread weathering processes were active in the region at the time of the late Proterozoic and had continued through the Ordovician.

The North Shore Volcanic Group exists as a 10 km package of rocks that were deposited over 11.2 million years (Paces and Miller, 1993; Davis and Green, 1997). Flows were deposited at a maximum rate of roughly 0.9 km per 1 million years, or an average of 1 mm per year subsidence rate. U-Pb dates on several of the stratigraphic units indicate flows may have remained exposed for hundreds of thousands to millions of years before burial by additional lava flows (Paces and Miller, 1993; Davis and Green, 1997; Fairchild et al., 2017).

Paleoshorelines of the cratonic sequences during the Phanerozoic have been mapped around the high-standing flows of the Mid-continent Rift in eastern and southern Minnesota. The uppermost units of the North Shore Volcanic Group, the Schroeder and Lutsen basalts, have no evidence of ever having been covered over for the vast majority of their history. It is likely that these superior rock units of the Midcontinent Rift have been exposed at the surface since their emplacement 1.09-1.083 billion (Fairchild et al., 2017) years ago until the Pleistocene glaciation.

During the late Proterozoic, the climate was considered to be tropical to subtropical (Turek and Robinson, 1984; Ojakangas et al., 2001a). Continental rifting is known to release massive amounts of CO_2 via tectonic degassing into the atmosphere (Lee et al, 2016; Brune et al., 2017). Weathering is readily facilitated by environments that are warm and wet with ample CO_2 for drawdown. It is therefore not unreasonable to assume that the rocks of the Mid-continent Rift were subject to significant surficial weathering activity during Midcontinent Rift formation.

Within the North Shore Volcanic Group, the Lafayette Bluff diabase sill at Crow Creek intruded into the surrounding Gooseberry River Basalts. The intrusion occurred at a depth of 3-5 km resulting in incipient metamorphism that produced chlorite, prehnite, and laumontite as the sill cooled. It is likely that some clays were present prior to burial from surficial *in situ* weathering. This burial would have facilitated the illitization of already formed smectite and possibly kaolinite observed in XRD scans through incipient metamorphism. Kaolinite in particular is associated with long periods of weathering suggesting more ancient origins (White and Brantley, 2003; Zhu, 2005; Zhu et al., 2006; Yuan et al., 2019).

Despite the existence of multiple clays including kaolinite, they were not observed in every sample, with kaolinite and illite observed only in vein material. This suggests that the Crow Creek site are the remains of the base of the saprolite profile. The removal of the upper portions of the profile can be reasonably assumed to have occurred during Pleistocene glaciation.

The Silver Bay granophyre is an intrusion into the surrounding diabase that was dated at 1094 Ma (Juda, 2006). The weathering of the granophyre was likely along a fracture through which warm circulating waters penetrated, facilitating the breakup of the rock. Water circulation continually deposited calcite, resulting in a higher concentration than the weathering of in situ minerals would produce. The presence of smectite and kaolinite suggests a similar history to the Crow Creek site of ancient weathering that was subsequently scraped away to the base by glaciation.

Several workers have suggested that prior to early Pleistocene glaciation, an extensive saprolite cover was present over North America (Chalmers, 1898; Clark and Pollard 1998; Bouchard and Jolicoeur, 2000; O'Beirne-Ryan and Zentilli, 2003; Jansson and Lidmar-Bergström, 2004; Zauyah et al., 2010). The sites in this study are exposures of weathered bedrock that is elsewhere in Minnesota covered by glacial sediment. The Crow Creek site is located approximately 20 miles to the southwest of the Silver Bay site. Drill cores throughout the state have recorded saprolite below till cover. Glacial tills in Kansas and Nebraska contain kaolinite suggested to have been assimilated during the erosion of saprolite. Clark and Pollard (1998) theorized the shift in glaciation cycles was due to the removal of this saprolite.

Schmidt et al. (2021) describe regional post-eruptive thermal alteration occurring over a timeframe of 107 million years that transitioned from close-to-surface to burial alteration. Surficial weathering of Midcontinent rift rocks subjected to burial conditions and magmatic intrusions produced an environment that allowed for the illitization of buried kaolinite and smectite and the formation of assemblages of prehnite-chlorite-laumontite.

There were multiple periods in the geologic history of these rocks where the climate was warm, wet, and had sufficient atmospheric CO2 to facilitate extensive weathering. The presence of kaolinite at both the Crow Creek and Silver Bay site suggests the weathering is particularly long-lived. The results of this study support the conclusions of prior research that an extensive and ancient weathering horizon once existed on the craton and has either been largely removed or covered by Pleistocene glaciation. The age of the weathering is difficult to determine, but weathering on the Shield has been the dominant geological environment at least since the Late Proterozoic about 750 Ma ago (Farley and McKeon, 2015), and likely much longer. Therefore, caution should be used when interpreting all of the saprolite in Minnesota as Mesozoic in age.

REFERENCES

Alderton, D. (2020). Other Silicates: The Al_2SiO_5 Polymorphs, Cordierite, Staurolite, Epidote, Chlorite. *Encyclopedia of Geology*, 378-380.

Altaner, S.P. (1978). Smectite group. *Encyclopedia of Sediments and Sedimentary Rocks. Encyclopedia of Earth Sciences Series*, 675-677.

Ansdell, K. M., Lucas, S. B., Connors, K., & Stern, R. A. (1995). Kisseynew metasedimentary gneiss belt, Trans-Hudson orogen (Canada): Back-arc origin and collisional inversion. *Geology*, *23*(11), 1039-1043.

Appelo, C. A. J., & Postma, D. (2004). *Geochemistry, groundwater and pollution*. CRC press, 649.

Baker, I., Haggerty, S.E. The alteration of olivine in basaltic and associated lavas. *Contr. Mineral. and Petrol.* 16, 258–273 (1967).

Bekker, A. (2015). Huronian glaciation. *Encyclopedia of Astrobiology*, 1128-1135.

Bohn, H. L., O'Connor, G. A., & Strawn, D. G. (2015). *Soil chemistry*. John Wiley & Sons.

Bouchard, M., & Jolicoeur, S. (2000). Chemical weathering studies in relation to geomorphological research in southeastern Canada. *Geomorphology*, *32*(3-4), 213-238.

Brune, S., Williams, S. E., & Mueller, R. D. (2017). Potential links between continental rifting, CO2 degassing and climate change through time. *Nature Geoscience*, *10*(12), 941-946.

Buol, S. W., & Weed, S. B. (1991). Saprolite-soil transformations in the Piedmont and Mountains of North Carolina. Geoderma, 51(1–4), 15–28.

Camuffo, Dario. (1995). Physical weathering of stones, Science of The Total Environment, Volume 167, Issues 1–3, Pages 1-14, ISSN 0048-9697.

Cannon, W. F. (1992). The Midcontinent rift in the Lake Superior region with emphasis on its geodynamic evolution. *Tectonophysics*, *213*(1-2), 41-48.

Cannon, W. F., LaBerge, G. L., Klasner, J. S., & Schulz, K. J. (2008). *The Gogebic iron range—A sample of the northern margin of the Penokean fold and thrust belt* (No. 1730). US Geological Survey.

Card, K. D. (1990). A review of the Superior Province of the Canadian Shield, a product of Archean accretion. *Precambrian research*, *48*(1-2), 99-156.

Chalmers, R. (1898). ART. XXXV.--The Pre-Glacial Decay of Rocks in Eastern Canada. *American Journal of Science (1880-1910)*, *5*(28), 273.

Cho, M., Liou, J.G., and Maruyama, S. (1986) Transition from zeolite to prehnite-pumpellyite facies in the Kartmutsen metabasites, Vancouver Island, British Columbia. *J. Petr*. 27, 467-494.

Ciborowski, T. J. R., Kerr, A. C., Ernst, R. E., McDonald, I., Minifie, M. J., Harlan, S. S., & Millar, I. L. (2015). The early proterozoic Matachewan large Igneous Province: Geochemistry, petrogenesis, and implications for earth evolution. *Journal of Petrology*, *56*(8), 1459-1494.

Clark, P. U., & Pollard, D. (1998). Origin of the middle Pleistocene transition by ice sheet erosion of regolith. *Paleoceanography*, *13*(1), 1-9.

Cocks, L. R. M., & Torsvik, T. H. (2011). The Palaeozoic geography of Laurentia and western Laurussia: a stable craton with mobile margins. *Earth-Science Reviews*, *106*(1-2), 1-51.

Colman, S. M. (1982). *Chemical weathering of basalts and andesites; evidence from weathering rinds United States Geological Survey Professional Paper* (No. 1246).

Craddock, J. P., Rainbird, R. H., Davis, W. J., Davidson, C., Vervoort, J. D., Konstantinou, A., ... & Lundquist, B. (2013). Detrital zircon geochronology and provenance of the Paleoproterozoic Huron (~ 2.4–2.2 Ga) and Animikie (~ 2.2–1.8 Ga) basins, southern Superior Province. *The Journal of Geology*, *121*(6), 623-644.

Craddock, J. P., Malone, D. H., Schmitz, M. D., & Gifford, J. N. (2018). Strain variations across the Proterozoic Penokean orogen, USA and Canada. *Precambrian Research*, *318*, 25-69.

Davis, D. W., & Green, J. C. (1997). Geochronology of the North American Midcontinent rift in western Lake Superior and implications for its geodynamic evolution. *Canadian Journal of Earth Sciences*, *34*(4), 476-488.

Davidson Jr, D. M. (1980). Emplacement and deformation of the Archean Saganaga batholith, Vermilion district, northeastern Minnesota. *Tectonophysics*, *66*(1-3), 179-195.

Dill, H. G. (2016). Kaolin: Soil, rock and ore: From the mineral to the magmatic, sedimentary and metamorphic environments. *Earth-Science Reviews*, *161*, 16-129.

Driese, S. G., Jirsa, M. A., Ren, M., Brantley, S. L., Sheldon, N. D., Parker, D., & Schmitz, M. (2011). Neoarchean paleoweathering of tonalite and metabasalt: Implications for reconstructions of 2.69 Ga early terrestrial ecosystems and paleoatmospheric chemistry. *Precambrian Research*, *189*(1-2), 1-17.

Dupré, B., Dessert, C., Oliva, P., Goddéris, Y., Viers, J., François, L., ... & Gaillardet, J. (2003). Rivers, chemical weathering and Earth's climate. Comptes Rendus Geoscience, 335(16), 1141-1160.Feininger, T. (1971). Chemical weathering and glacial erosion of crystalline rocks and the origin of till. US Geological Survey Professional Paper, 750, C65-C81.

Earle, S. (2015). *Physical geology*. BCcampus.

Eriksson, P. G., & Condie, K. C. (2014). Cratonic sedimentation regimes in the ca. 2450–2000 Ma period: relationship to a possible widespread magmatic slowdown on Earth?. *Gondwana Research*, *25*(1), 30-47.

Eyles, N., & Januszczak, N. (2004). 'Zipper-rift': a tectonic model for Neoproterozoic glaciations during the breakup of Rodinia after 750 Ma. *Earth-Science Reviews*, *65*(1-2), 1-73.

Fairchild, L. M., Swanson-Hysell, N. L., Ramezani, J., Sprain, C. J., & Bowring, S. A. (2017). The end of Midcontinent Rift magmatism and the paleogeography of Laurentia. *Lithosphere*, *9*(1), 117-133.

Farley, K. A., & McKeon, R. (2015). Radiometric dating and temperature history of banded iron formation–associated hematite, Gogebic iron range, Michigan, USA. *Geology*, *43*(12), 1083-1086.

Fedo, C. M., Young, G. M., & Nesbitt, H. W. (1997). Paleoclimatic control on the composition of the Paleoproterozoic Serpent Formation, Huronian Supergroup, Canada: a greenhouse to icehouse transition. *Precambrian Research*, *86*(3-4), 201-223.

Fix, P. M. (2015). *Characterization of Weathering Products on Duluth Complex Rocks and Implications for Metal Mobility, Mesaba Deposit, Minnesota, USA* (Doctoral dissertation, University of Minnesota).

Flint, R. F. (1971). Glacial and Quaternary geology. 114-121.

Frost, B. R. (1980). Observations on the boundary between zeolite facies and prehnite-pumpellyite facies. *Contributions to mineralogy and petrology*, *73*(4), 365-373.

Frost, B. R., & Beard, J. S. (2007). On silica activity and serpentinization. *Journal of petrology*, *48*(7), 1351-1368.

Fulignati P. Clay Minerals in Hydrothermal Systems. *Minerals.* 2020; 10(10), 919.

Gehman JR, H. M. (1957). The petrology of the Beaver Bay Complex, Lake County, Minnesota. University of Minnesota.

Geul, J. J. C. (1970). Geology of Devon and Pardee townships and the Stuart location, District of Thunder Bay. Ontario Department of Mines.

Gibbard, P. L., Head, M. J., Walker, M. J., & Subcommission on Quaternary Stratigraphy. (2010). Formal ratification of the Quaternary System/Period and the Pleistocene Series/Epoch with a base at 2.58 Ma. *Journal of Quaternary Science*, *25*(2), 96-102.

Goldich, S. S. (1938). A Study in Rock Weathering: Journal of Geology, 46, 17-58.

Grant, J. A. (1986). The isocon diagram; a simple solution to Gresens' equation for metasomatic alteration. *Economic geology*, *81*(8), 1976-1982.

Grant, J. A. (2005). Isocon analysis: A brief review of the method and applications. *Physics and Chemistry of the Earth, Parts A/B/C*, *30*(17-18), 997-1004.

Green, J. C. (1972). General geology, northeastern Minnesota. North Shore Volcanic Group. Geology of Minnesota, a centennial volume., 422-487.

Green, J. C. (1989). Physical volcanology of mid-Proterozoic plateau lavas: The Keweenawan North Shore Volcanic Group, Minnesota. Geological Society of America Bulletin, 101, 486-500.

Green, J. C. (1996). *Geology on Display: Geology and Scenery of Minnesota's North Shore State Parks*. Minn. Department of Natural Resources.

Grogan, R. M., (1940). Geology of a Part of the Minnesota Shore of Lake Superior Northeast of Two Harbors, Minnesota; unpublished Ph. D. thesis, Univ. of Minnesota, 110 p.

Hall, A. M., Ebert, K., & Hättestrand, C. (2013). Pre-glacial landform inheritance in a glaciated shield landscape. *Geografiska Annaler: Series A, Physical Geography*, *95*(1), 33-49.

Hallberg, G. R. (1980). Illinoian and Pre-Illinoian stratigraphy of southeast Iowa and adjacent Illinois.

Halls, H. C., & Zhang, B. (1998). Uplift structure of the southern Kapuskasing zone from 2.45 Ga dike swarm displacement. *Geology*, *26*(1), 67-70.

Halls, H. C., Davis, D. W., Stott, G. M., Ernst, R. E., & Hamilton, M. A. (2008). The Paleoproterozoic Marathon Large Igneous Province: New evidence for a 2.1 Ga long-lived mantle plume event along the southern margin of the North American Superior Province. *Precambrian Research*, *162*(3-4), 327-353.

Harnois, L., & Moore, J. M. (1988). Geochemistry and origin of the Ore Chimney Formation, a transported paleoregolith in the Grenville Province of southeastern Ontario, Canada. *Chemical Geology*, *69*(3-4), 267-289.

Herndon, E. M., Jin, L., & Brantley, S. L. (2011). Soils reveal widespread manganese enrichment from industrial inputs. *Environmental science & technology*, *45*(1), 241-247.

Hinze, W. J., & Chandler, V. W. (2020). Reviewing the configuration and extent of the Midcontinent rift system. *Precambrian Research*, *342*, 105688.

Hoffman, A. T. (2007). Lithostratigraphy, Hydrothermal Alteration, and Lithogeochemistry of Neoarchean Rocks in the Lower and Soudan Member of the Ely Greenstone Formation, Vermilion District, Northeastern Minnesota: Implications for Volcanogenic Massive Sulfides.

Hoinkes, G., Hauzenberger, C. A., & Schmid, R. (2005). METAMORPHIC ROCKS | Classification, Nomenclature and Formation. *Encyclopedia of Geology, Volumes 1-5, 386-402.*

Hollings, P., Smyk, M., Halls, H., & Heaman, L. (2010). The geochemistry, paleomagnetism and geochronology of the dykes and sills associated with the Midcontinent Rift near Thunder Bay, Ontario, Canada. Precambrian Research, 183, 553-571.

Holm, D., Medaris Jr, L. G., McDannell, K. T., Schneider, D. A., Schulz, K., Singer, B. S., & Jicha, B. R. (2020). Growth, overprinting, and stabilization of Proterozoic Provinces in the southern Lake Superior region. *Precambrian Research*, *339*, 105587.

Huang, P. M., & Wang, M. K. (2005). Minerals, Primary. *Encyclopedia of Soils in the Environment, Volume 2*, 500-510.

Huggett, J. M. (2005). Clays and Their Diagenesis. *Encyclopedia of Geology, Volumes 1-5*, 65-69.

Iijima, A. and Utada, M. (1972) Zeolitic zoning of the Neogene pyroclastic rocks in Japan. *Japan. J. Geol. Geog.* 42, 61-83.

Jansson, K. N., & Lidmar-Bergström, K. (2004). Observations on weathering forms at the Caniapiscau Reservoir, North-Central Québec, Canada. *Canadian Geographer/Le Géographe canadien*, *48*(1), 1-10.

Jaupart, C., Mareschal, J. C., Bouquerel, H., & Phaneuf, C. (2014). The building and stabilization of an Archean Craton in the Superior Province, Canada, from a heat flow perspective. *Journal of Geophysical Research: Solid Earth*, *119*(12), 9130-9155.

Jirsa, M. A., Miller Jr, J. D., & Morey, G. B. (2008). Geology of the Biwabik iron formation and Duluth complex. *Regulatory Toxicology and Pharmacology*, *52*(1), S5-S10.

Jirsa, M. A., Boerboom, T. J., Green, J. C., Miller Jr, J. D., Morey, G. B., Ojakangas, R. W., Peterson, D. M. & Severson, M. J.(2004). FIELD TRIP 5--CLASSIC OUTCROPS OF NORTHEASTERN MINNESOTA.

Johnson, T. A., Vervoort, J. D., Ramsey, M. J., Southworth, S., & Mulcahy, S. R. (2020). Tectonic evolution of the Grenville Orogen in the central Appalachians. *Precambrian Research*, *346*, 105740.

Karathanasis, A. D., & Hajek, B. F. (1983). Transformation of smectite to kaolinite in naturally acid soil systems: Structural and thermodynamic considerations. Soil Science Society of America Journal, 47(1), 158-163.

Karlstrom, K. E., Harlan, S. S., Williams, M. L., McLelland, J., Geissman, J. W., & Ahall, K. I. (1999). Refining Rodinia: Geologic evidence for the Australia–western US connection in the Proterozoic. *GSA Today*, *9*(10), 1-7.

Karlstrom, K., Hagadorn, J., Gehrels, G., Matthews, W., Schmitz, M., Madronich, L., Mulder, J., Pecha, M., Giesler, D., & Crossey, L. (2018). Cambrian Sauk transgression in the Grand Canyon region redefined by detrital zircons. *Nature Geoscience*, *11*(6), 438-443.

Klein, G. D. V. (1991). Origin and evolution of North American cratonic basins. *South African journal of geology*, *94*(1), 3-18.

Klein, C. (2005). Some Precambrian banded iron-formations (BIFs) from around the world: Their age, geologic setting, mineralogy, metamorphism, geochemistry, and origins. *American Mineralogist*, *90*(10), 1473-1499.

Kloprogge, J. T., Komarneni, S., & Amonette, J. E. (1999). Synthesis of smectite clay minerals: a critical review. *Clays and Clay Minerals*, *47*, 529-554.

Krabbendam, M., & Bradwell, T. (2014). Quaternary evolution of glaciated gneiss terrains: Pre-glacial weathering vs. glacial erosion. Quaternary Science Reviews, 95, 20–42.

Kretzschmar, R., Robarge, W. P., Amoozegar, A., & Vepraskas, M. J. (1997). Biotite alteration to halloysite and kaolinite in soil-saprolite profiles developed from mica schist and granite gneiss. Geoderma, 75(3–4), 155–170.

Kronberg, B. I., Nesbitt, H. W., & Lam, W. W. (1986). Upper Pleistocene Amazon deep-sea fan muds reflect intense chemical weathering of their mountainous source lands. *Chemical Geology*, *54*(3-4), 283-294.

Kuethe, J.R.. (2016). The classification of eclogites and how the role of fluids, mineralogy and chemistry helps to determine their processes of formation.

Lamadrid, H. M., Rimstidt, J. D., Schwarzenbach, E. M., Klein, F., Ulrich, S., Dolocan, A., & Bodnar, R. J. (2017). Effect of water activity on rates of serpentinization of olivine. *Nature Communications*, *8*(1), 16107.

Larson, P. C. (2008). Sediment transport cycles of the Laurentide Ice Sheet.

Lee, H., Muirhead, J. D., Fischer, T. P., Ebinger, C. J., Kattenhorn, S. A., Sharp, Z. D., & Kianji, G. (2016). Massive and prolonged deep carbon emissions associated with continental rifting. *Nature Geoscience*, *9*(2), 145-149.

Lepp, H., & Goldich, S. S. (1964). Origin of Precambrian iron formations. *Economic Geology*, *59*(6), 1025-1060.

Levin, H. L., & King Jr, D. T. (2016). *The Earth through time*. John Wiley & Sons. 282-286.

Li, Z. X., Evans, D. A., & Halverson, G. P. (2013). Neoproterozoic glaciations in a revised global palaeogeography from the breakup of Rodinia to the assembly of Gondwanaland. *Sedimentary Geology*, *294*, 219-232.

Lidmar-Bergström, K. (1995). Relief and saprolites through time on the Baltic Shield. *Geomorphology*, *12*(1), 45-61.

Lidmar-Bergström, K. (1997). A long-term perspective on glacial erosion. *Earth Surface Processes and Landforms: The Journal of the British Geomorphological Group*, *22*(3), 297-306.

Lin, S., Parks, J., Heaman, L. M., Simonetti, A., & Corkery, M. T. (2013). Diapirism and sagduction as a mechanism for deposition and burial of "Timiskaming-type" sedimentary sequences, Superior Province: Evidence from detrital zircon geochronology and implications for the Borden Lake conglomerate in the exposed middle to lower crust in the Kapuskasing uplift. *Precambrian Research*, *238*, 148-157.

Lodge, R. W., Gibson, H. L., Stott, G. M., Hudak, G. J., Jirsa, M. A., & Hamilton, M. A. (2013). New U–Pb geochronology from Timiskaming-type assemblages in the Shebandowan and Vermilion greenstone belts, Wawa subprovince, Superior Craton: Implications for the Neoarchean development of the southwestern Superior Province. *Precambrian Research*, *235*, 264-277.

Machado, N., Zwanzig, H., & Parent, M. (2000). U–Pb ages of plutonism, sedimentation, and metamorphism of the Paleoproterozoic Kisseynew metasedimentary belt, Trans-Hudson Orogen (Manitoba, Canada). *Canadian Journal of Earth Sciences*, *36*(11), 1829-1842.

Maher, K., DePaolo, D. J., Lin, J.C.F. (2004). Rates of silicate dissolution in deep-sea sediment: in situ measurement using U-234/U-238 of pore fluids. Geochimica et Cosmochimica Acta, 68 (22) 4629-4648.

Mantovani, M., Escudero, A., & Becerro, A. I. (2010). Effect of pressure on kaolinite illitization. *Applied Clay Science*, *50*(3), 342-347.

Medaris Jr, L. G., Jicha, B. R., Singer, B. S., Wathen, B., Li, Y., & Driese, S. G. (2022). Evaluating the Magnitudes of Weathering and Potassium Metasomatism in Paleosols: Examples from Proterozoic, Cambrian, and Cretaceous Paleosols in Midcontinental Laurentia. *The Journal of Geology*, *130*(6), 000-000.

Miller, J.D., Ripley, E.M. (1996). Layered Intrusions of the Duluth Complex, Minnesota, USA, Developments in Petrology, 15, Pages 257-301.

Miller, J. D., & Chandler, V. W. (1997). Geology, petrology, and tectonic significance of the Beaver Bay Complex, northeastern Minnesota. Geological Society of America Special Papers, 312, 73-96.

Miller, J. D., Nicholson, S. W., Easton, R. M., Ripley, E. M., & Feinberg, J. M. (2013). Geology and mineral deposits of the 1.1 Ga Midcontinent Rift in the Lake Superior region—An overview. *Field guide to the copper-nickel-platinum group element deposits of the Lake Superior Region. Edited by Miller, J. Precambrian Research Center Guidebook*, *13*(01), 1-49.

Minnesota Department of Transportation (2013). MnDOT Geotechnical Manual Appendix A - Geology of Minnesota.

Minnesota Well Index , (2023), Minnesota Department of Health, https://www.health.state.mn.us/communities/environment/water/mwi/index.html

Mitchell, R. L., & Sheldon, N. D. (2009). Weathering and paleosol formation in the 1.1 Ga Keweenawan Rift. *Precambrian Research*, *168*(3-4), 271-283.

Mooers, H. D., & Lehr, J. D. (1997). Terrestrial record of Laurentide Ice Sheet reorganization during Heinrich events. *Geology*, *25*(11), 987-990.

Moore, D. E., & Rymer, M. J. (2007). Talc-bearing serpentinite and the creeping section of the San Andreas fault. *Nature*, *448*(7155), 795-797.

Morey, G. B. (1978). RI-21 Lower and Middle Precambrian Stratigraphic Nomenclature for East-Central Minnesota.

Morey, G. B. (1980). A brief review of the geology of the western Vermilion district, northeastern Minnesota. *Precambrian Research*, *11*(3-4), 247-265.

Morris, W. A. (1977). Paleolatitude of glaciogenic upper Precambrian Rapitan Group and the use of tillites as chronostratigraphic marker horizons. *Geology*, *5*(2), 85-88.

Mossman, D., Eigendorf, G., Tokaryk, D., Gauthier-Lafaye, F., Guckert, K. D., Melezhik, V., & Farrow, C. E. (2003). Testing for fullerenes in geologic materials: Oklo carbonaceous substances, Karelian shungites, Sudbury Black Tuff. *Geology*, *31*(3), 255-258.

Mueller, W., & Donaldson, J. A. (1992). Development of sedimentary basins in the Archean Abitibi belt, Canada: an overview. *Canadian Journal of Earth Sciences*, *29*(10), 2249-2265.

Nelson, D. R. (1998). Granite–greenstone crust formation on the Archaean Earth: a consequence of two superimposed processes. *Earth and Planetary Science Letters*, *158*(3-4), 109-119.

Nesbitt, H. W., & Wilson, R. E. (1992). Recent chemical weathering of basalts. *American Journal of science*, *292*(10), 740-777.

Nesbitt, H., & Young, G. M. (1982). Early Proterozoic climates and plate motions inferred from major element chemistry of lutites. *nature*, *299*(5885), 715-717.

O'Beirne-Ryan, A. M., & Zentilli, M. (2003). Paleoweathered surfaces on granitoids of southern Nova Scotia: paleoenvironmental implications of saprolites. *Canadian Journal of Earth Sciences*, *40*(6), 805-817.

Ojakangas, R. W., Morey, G. B., & Green, E. C. (2001a). The Mesoproterozoic midcontinent rift system, Lake Superior region, USA. *Sedimentary Geology*, *141*, 421-442.

Ojakangas, R. W., Morey, G. B., & Southwick, D. L. (2001b). Paleoproterozoic basin development and sedimentation in the Lake Superior region, North America. *Sedimentary Geology*, *141*, 319-341.

Ojakangas, R. W., Severson, M. J., & Jongewaard, P. K. (2011). Geology and sedimentology of the Paleoproterozoic Animikie group: the Pokegama formation, the Biwabik Iron formation, and Virginia formation of the eastern Mesabi Iron range and Thomson formation near Duluth, northeastern Minnesota.

Olvmo, M., Lidmar-Bergström, K., Ericson, K., & Bonow, J. M. (2005). Saprolite remnants as indicators of pre-glacial landform genesis in southeast sweden. *Geografiska Annaler: Series A, Physical Geography*, *87*(3), 447-460.

Paces, J. B., & Miller Jr, J. D. (1993). Precise U-Pb ages of Duluth complex and related mafic intrusions, northeastern Minnesota: Geochronological insights to physical, petrogenetic, paleomagnetic, and tectonomagmatic processes associated with the 1.1 Ga midcontinent rift system. *Journal of Geophysical Research: Solid Earth*, *98*(B8), 13997-14013.

Parham, W. E. (1970). SP-10 Clay mineralogy and geology of Minnesota's kaolin clays.

Patterson, C. J., & Boerboom, T. J. (1999). The significance of pre-existing, deeply weathered crystalline rock in interpreting the effects of glaciation in the Minnesota River valley, USA. *Annals of Glaciology*, *28*, 53-58.

Percival, J. A. (2007). Geology and metallogeny of the Superior Province, Canada. In *Mineral deposits of Canada: A synthesis of major deposit-types, district metallogeny, the evolution of geological provinces, and exploration methods* (Vol. 5, pp. 903-928). Geological Association of Canada, Mineral Deposits Division. Special Publication No. 5.

Percival, J. A., Skulski, T., Sanborn-Barrie, M., Stott, G. M., Leclair, A. D., Corkery, M. T., & Boily, M. (2012). Geology and tectonic evolution of the Superior Province, Canada. In *Tectonic styles in Canada: The LITHOPROBE perspective* (Vol. 49, pp. 321-378). Special Paper 49: Geological Association of Canada.

Pope, N. M. (1976). Petrology and structure of the late Precambrian mafic sills east of Silver Creek, Lake County, Minnesota.

Poulton, S. W., Fralick, P. W., & Canfield, D. E. (2010). Spatial variability in oceanic redox structure 1.8 billion years ago. *Nature Geoscience*, *3*(7), 486-490.

Purucker, M. (1983). Time of formation of soft iron ore on the Gunflint and Mesabi Ranges (Ontario, Canada and Minnesota, USA). *Economic Geology*, *78*(3), 502-506.

Qin, X., Han, D. H., & Zhao, L. (2019). Elastic characteristics of overpressure due to smectite-to-illite transition based on micromechanism analysis. *Geophysics*, *84*(4), WA23-WA42.

Rainbird, R. H., Nesbitt, H. W., & Donaldson, J. A. (1990). Formation and diagenesis of a sub-Huronian saprolith: comparison with a modern weathering profile. *The Journal of Geology*, *98*(6), 801-822.

Rani, N., Shrivastava, J. P., & Bajpai, R. K. (2016). Long-term performance assessment of nuclear waste and natural glasses in the geological repository: a geochemical modelling. *Current Science*, *110*(2), 214.

Retallack, G. (1986). Reappraisal of a 2200 Ma-old paleosol near Waterval Onder, South Africa. *Precambrian Research*, *32*(2-3), 195-232.

Riebe, Clifford, S., Kirchner, James, W., Granger, Darryl, E., Finkel, Robert, C. (2001). Strong tectonic and weak climactic control of long-term chemical weathering rates. Geology, 29, 511-514.

Robertson, J. A., & Card, K. D. (1972). *Geology and Scenery: North Shore of Lake Huron Region* (No. 4). Ontario Ministry of Natural Resources, Division of Mines.

Rooney, A. D., Macdonald, F. A., Strauss, J. V., Dudás, F. Ö., Hallmann, C., & Selby, D. (2014). Re-Os geochronology and coupled Os-Sr isotope constraints on the Sturtian snowball Earth. *Proceedings of the National Academy of Sciences*, *111*(1), 51-56.

Roy, M., Clark, P. U., Raisbeck, G. M., & Yiou, F. (2004). Geochemical constraints on the regolith hypothesis for the middle Pleistocene transition. *Earth and Planetary Science Letters*, *227*(3-4), 281-296.

Roy, S. (1997). Genetic diversity of manganese deposition in the terrestrial geological record. *Geological Society, London, Special Publications*, *119*(1), 5-27.

Runkel, A. C., Miller, J. F., McKay, R. M., Palmer, A. R., & Taylor, J. F. (2007). High-resolution sequence stratigraphy of lower Paleozoic sheet sandstones in central North America: The role of special conditions of cratonic interiors in development of stratal architecture. *Geological Society of America Bulletin*, 119(7-8), 860-881.

Rutter, N. W. (1980). *Erosion by pleistocene continental ice sheets in the area of the Canadian Shield* (No. INFO--0014). Atomic Energy Control Board.

Sandberg, A. E., (1938). Section across Keweenawan lavas at Duluth, Minnesota. *Geological Society of America Bulletin*, v. 49, p. 795 - 830.

Schmidt, S. T., Süssenberger, A., Wemmer, K., & Steele-MacInnes, M. (2021). Posteruptive Thermal History of the Proterozoic Basaltic North Shore Volcanic Group of the Midcontinent Rift: Evidence from K/Ar Data of Celadonite. *Lithosphere*, *2021*(1).

Schulz, K. J., & Cannon, W. F. (2007). The Penokean orogeny in the Lake Superior region. *Precambrian Research*, *157*(1-4), 4-25.

Schwartz, S., Guillot, S., Reynard, B., Lafay, R., Debret, B., Nicollet, C., ... & Auzende, A. L. (2013). Pressure–temperature estimates of the lizardite/antigorite transition in high pressure serpentinites. *Lithos*, *178*, 197-210.

Seifert, Karl E. and Anderson, Raymond R. (1996) Geochemistry of Buried Midcontinent Rift Volcanic Rocks in Iowa: Data From Well Samples. *Journal of the Iowa Academy of Science: JIAS*, *103*(3-4), 63-73.

Sekine, Y., Tajika, E., Ohkouchi, N., Ogawa, N. O., Goto, K., Tada, R., ... & Yamamoto, S. (2007, December). Large negative excursion of organic carbon isotope in the aftermath of the Paleoproterozoic glaciation in North America: methane-hydrate destabilization, climate recovery, and the Great Oxidation Event. In *AGU Fall Meeting Abstracts* (Vol. 2007, pp. PP43B-1244).

Setterholm, D. R., & Morey, G. B. (1995). An extensive pre-Cretaceous weathering profile in east-central and southwestern Minnesota (No. 1989). US Department of the Interior, US Geological Survey.

Sims, P. K., & Morey, G. B. (1972). Geology of Minnesota: A centennial volume. Minnesota Geological Survey.

Sims, P. K. (1976). Early Precambrian tectonic-igneous evolution in the Vermilion district, northeastern Minnesota. *Geological Society of America Bulletin*, *87*(3), 379-389.

Slagstad, T., Roberts, N. M., & Kulakov, E. (2017). Linking orogenesis across a supercontinent; the Grenvillian and Sveconorwegian margins on Rodinia. *Gondwana Research*, *44*, 109-115.

Sloan, R. E. (1964). The Cretaceous System in Minnesota. Minnesota Geological Survey Report of Investigations 5, 72 pp.

Sloss, L. L. (Ed.). (1988). *Sedimentary Cover—North American Craton: US*. Geological Society of America.

Southwick, D. L., Welsh, J. L., Englebert, J. A., & Hauck, S. A. (1991). *Bedrock Geochemistry of Archean Rocks in Northern Minnesota*. University of Minnesota Duluth.

Strakhov, N. 1967. Principles of Lithogenesis. Oliver and Boyd, London.

Swanson-Hysell, N. L., Ramezani, J., Fairchild, L. M., & Rose, I. R. (2019). Failed rifting and fast drifting: Midcontinent Rift development, Laurentia's rapid motion and the driver of Grenvillian orogenesis. *GSA Bulletin*, *131*(5-6), 913-940.

Taner, M. F., & Chemam, M. (2015). Algoma-type banded iron formation (BIF), Abitibi Greenstone belt, Quebec, Canada. *Ore geology reviews*, *70*, 31-46.

Thompson, A. R. (2015). A hydrothermal model for metasomatism of neoarchean Algoma-Type banded iron formation to massive hematite ore at the Soudan Mine, NE Minnesota.

Tschernich, R. (1992) Zeolites of the world. Geoscience Press Inc., Phoenix, AZ, USA, 563 pages.

Turek, A. and Robinson, R.N. (1984). Geology of the Precambrian Basement in Southern Ontario, Ontario Geological Survey Open File Report 5496, 135p., 6 appendices, numerous maps and figures.

Upham, W. (1904). Boulders Due to Rock Decay. *The American Geologist*, *33*, 370.

Vallini, D. A., Cannon, W. F., & Schulz, K. J. (2006). Age constraints for Paleoproterozoic glaciation in the Lake Superior Region: detrital zircon and hydrothermal xenotime ages for the Chocolay Group, Marquette Range Supergroup. *Canadian Journal of Earth Sciences*, *43*(5), 571-591.

Velbel, M. A., & Barker, W. W. (2008). Pyroxene weathering to smectite: conventional and cryo-field emission scanning electron microscopy, Koua Bocca ultramafic complex, Ivory Coast. *Clays and Clay Minerals*, *56*(1), 112-127.

Vervoort, J. D. (1987). Petrology and geochemistry of the Archean rocks of the Jap Lake area, northeastern Minnesota.

Wahl, T. E. (2007). Geology and mineral potential of the Duluth Complex and related rocks of northeastern Minnesota: Minnesota Geological Survey Report of Investigation 58, 207p. Miller, JD.

Walker, M., Head, M. J., Lowe, J., Berkelhammer, M., BjÖrck, S., Cheng, H., ... & Weiss, H. (2019). Subdividing the Holocene Series/Epoch: formalization of stages/ages and subseries/subepochs, and designation of GSSPs and auxiliary stratotypes. *Journal of Quaternary Science*, *34*(3), 173-186.

Weller, O. M., & St-Onge, M. R. (2017). Record of modern-style plate tectonics in the Palaeoproterozoic Trans-Hudson orogen. *Nature Geoscience*, *10*(4), 305-311.

White, A. F., Brantley, S. L., (1995) Chemical Weathering Rates of Silicate Minerals, *Mineralogical Society of America*, pp. 1-22

White, A. F., & Brantley, S. L. (2003). The effect of time on the weathering of silicate minerals: why do weathering rates differ in the laboratory and field?. *Chemical Geology*, *202*(3-4), 479-506.

Williams, G. E., Schmidt, P. W., & Young, G. M. (2016). Strongly seasonal Proterozoic glacial climate in low palaeolatitudes: Radically different climate system on the pre-Ediacaran Earth. *Geoscience Frontiers*, *7*(4), 555-571.

Winchell, N. H. (1900). *1872-[1901] The Geology of Minnesota: Vol. I [-VI] of the Final Report* (Vol. 5). Pioneer Press Company, printers.

Wilson, M. J. (2004). Weathering of the primary rock-forming minerals: processes, products and rates. *Clay Minerals*, *39*(3), 233-266.

Xiao, M., Yuan, X., Cheng, D., Wu, S., Cao, Z., Tang, Y., & Xie, Z. (2018). Feldspar dissolution and its influence on reservoirs: a case study of the Lower Triassic Baikouquan Formation in the northwest margin of the Junggar Basin, China. *Geofluids*, *2018*.

Young, G. M. (2002). Stratigraphic and tectonic settings of Proterozoic glaciogenic rocks and banded iron-formations: relevance to the snowball Earth debate. *Journal of African Earth Sciences*, *35*(4), 451-466.

Young, G. M. (2013). Precambrian supercontinents, glaciations, atmospheric oxygenation, metazoan evolution and an impact that may have changed the second half of Earth history. *Geoscience Frontiers*, *4*(3), 247-261.

Young, G. M. (2015). Did prolonged two-stage fragmentation of the supercontinent Kenorland lead to arrested orogenesis on the southern margin of the Superior province?. *Geoscience Frontiers*, *6*(3), 419-435.

Young, G. M. (2019). Aspects of the Archean-Proterozoic transition: How the great Huronian Glacial Event was initiated by rift-related uplift and terminated at the rift-drift transition during break-up of Lauroscandia. *Earth-Science Reviews*, *190*, 171-189.

Yuan, G., Cao, Y., Schulz, H. M., Hao, F., Gluyas, J., Liu, K., ... & Li, F. (2019). A review of feldspar alteration and its geological significance in sedimentary basins: From shallow aquifers to deep hydrocarbon reservoirs. *Earth-science reviews*, *191*, 114-140.

Zauyah, S., Schaefer, C. E., & Simas, F. N. (2010). Saprolites. In *Interpretation of micromorphological features of soils and regoliths* (pp. 49-68). Elsevier.

Zhao, Guochun (2021). Metamorphism of Mafic Rocks. *Encyclopedia of Geology (Second Edition)*, 457-464.

Zhu, C. (2005). In situ feldspar dissolution rates in an aquifer. *Geochimica et Cosmochimica Acta*, *69*(6), 1435-1453.

Zhu, C., Veblen, D. R., Blum, A. E., & Chipera, S. J. (2006). Naturally weathered feldspar surfaces in the Navajo Sandstone aquifer, Black Mesa, Arizona: Electron microscopic characterization. *Geochimica et Cosmochimica Acta*, *70*(18), 4600-4616.